

MANITOBA

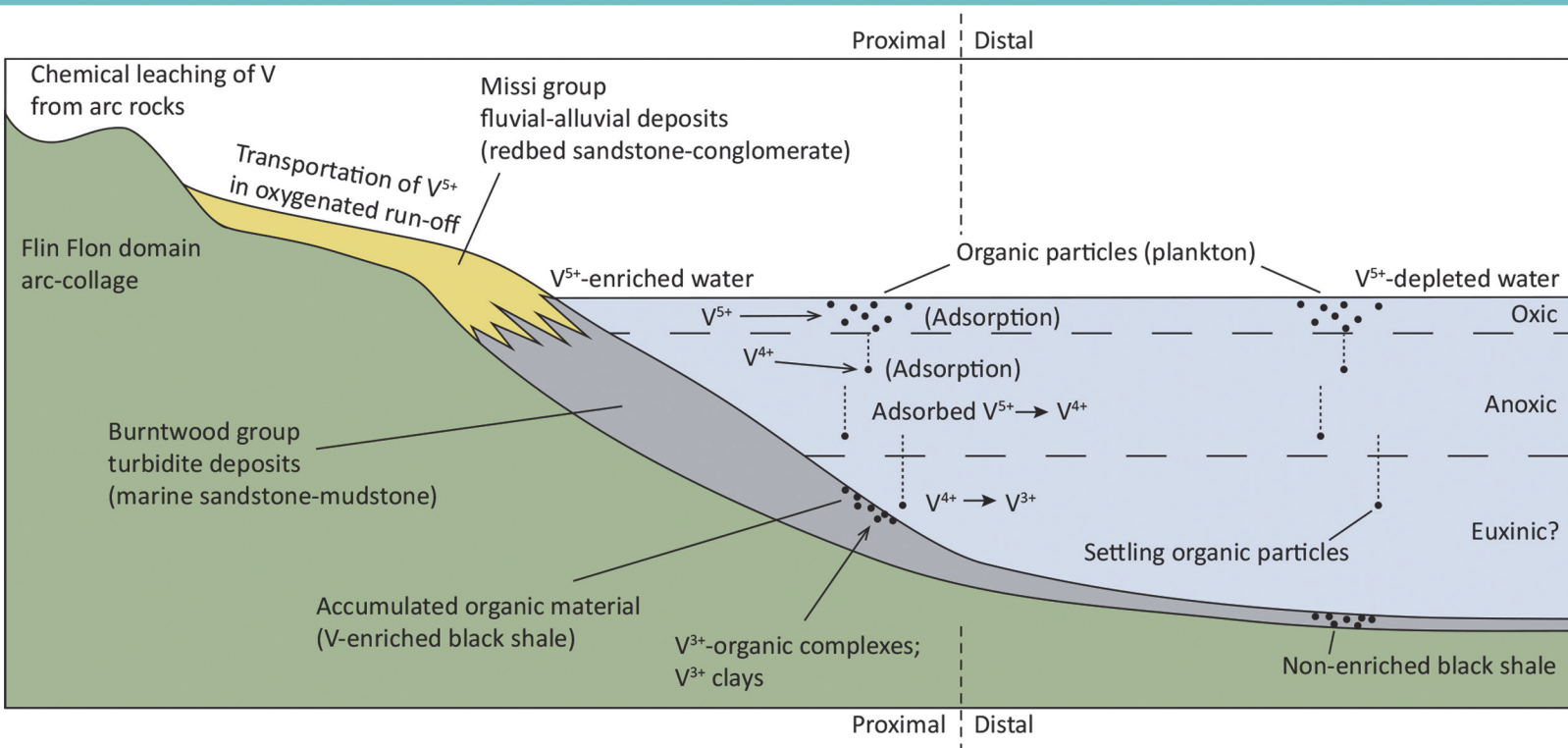
INVEST. BUILD. GROW.



GEOSCIENTIFIC PAPER GP2020-1

GEOLOGY AND INTERPRETATION OF GRAPHITE- AND VANADIUM-ENRICHED DRILLCORE FROM THE HUZYK CREEK PROPERTY, SUB-PHANEROZOIC KISSEYNEW DOMAIN, CENTRAL MANITOBA (NTS 63J6)

Manitoba Geological Survey





Geoscientific Paper GP2020-1

**Geology and interpretation of graphite- and
vanadium-enriched drillcore from the Huzyk Creek
property, sub-Phanerozoic Kisseynew domain,
central Manitoba (NTS 63J6)**

**by C.G. Couëslan
Manitoba Geological Survey
Winnipeg, 2020**

©Queen's Printer for Manitoba, 2020

Every possible effort is made to ensure the accuracy of the information contained in this report, but Manitoba Agriculture and Resource Development does not assume any liability for errors that may occur. Source references are included in the report and users should verify critical information.

Any third party digital data and software accompanying this publication are supplied on the understanding that they are for the sole use of the licensee, and will not be redistributed in any form, in whole or in part. Any references to proprietary software in the documentation and/or any use of proprietary data formats in this release do not constitute endorsement by Manitoba Agriculture and Resource Development of any manufacturer's product.

When using information from this publication in other publications or presentations, due acknowledgment should be given to the Manitoba Geological Survey. The following reference format is recommended:

Couëslan, C.G. 2020: Geology and interpretation of graphite- and vanadium-enriched drillcore from the Huzyk Creek property, sub-Phanerozoic Kisseynew domain, central Manitoba (NTS 63J6); Manitoba Agriculture and Resource Development, Manitoba Geological Survey, Geoscientific Paper GP2020-1, 29 p.

NTS grid: 63J6

Published by:

Manitoba Agriculture and Resource Development
Manitoba Geological Survey
360–1395 Ellice Avenue
Winnipeg, Manitoba
R3G 3P2 Canada

Telephone: 1-800-223-5215 (General Enquiry)
204-945-6569 (Publication Sales)

Fax: 204-945-8427

E-mail: minesinfo@gov.mb.ca

Website: manitoba.ca/minerals

ISBN: 978-0-7711-1606-3

This publication is available to download free of charge at manitoba.ca/minerals

Cover illustration:

Depositional model for the formation of the V-enriched graphite deposit at the Huzyk Creek property.

Abstract

Two drillcores intersect vanadium-enriched graphite schist in the Huzyk Creek area south of Ponton, Manitoba. The area is situated near the boundary between the sub-Phanerozoic Kiseynew domain and the Thompson nickel belt. The drillcore consists of a hornblende gneiss and calcsilicate package in contact, and locally interleaved, with a mudstone-wacke suite containing the graphite-rich horizon. The entire sequence is intruded by several types of felsic intrusions, and metamorphosed to lower granulite-facies conditions of approximately 5.6–7.3 kbar and 750–810°C. The wacke-mudstone package appears to be related to the Burntwood group of the Kiseynew domain, and was likely deposited relatively proximal to the Flin Flon arc-collage. The hornblende gneiss and calcsilicate are interpreted as variably altered mafic rocks, possibly basalt, and may be related to Missi-age, successor-arc magmatism. A model is proposed in which oxygenated surface run-off draining the Flin Flon arc-collage was enriched in vanadium. The run-off discharged into the anoxic Kiseynew basin where relatively mobile V^{5+} was reduced to less mobile V^{4+} , and adsorbed to organic matter. Settling of the organic particles into likely euxinic bottom waters further reduced the vanadium to relatively immobile V^{3+} . Upon burial and metamorphism, the organic-rich deposits were transformed into V-enriched graphitic horizons in the wacke-mudstone package. The model suggests that vanadium would be fractionated from the water shortly after discharge into the anoxic Kiseynew basin, and that graphitic horizons in relative close proximity to the Flin Flon arc-collage have a greater potential for vanadium enrichment.

Résumé

Deux carottes de forage croisent un schiste graphite enrichi en vanadium dans la région du site Huzyk Creek au sud de Ponton, au Manitoba. La région est située près de la limite entre la portion subphanérozoïque du Domaine de Kiseynew et la ceinture de nickel de Thompson. La carotte de forage est composée d'un ensemble de gneiss à hornblende et de silicate calcique en contact, et imbriqué par endroit, d'une combinaison de mudstone et de wacke contenant l'horizon riche en graphite. La totalité de la séquence est infiltrée par plusieurs types d'intrusions felsiques, et est métamorphisée dans des conditions de faciès des granulites plus faibles d'environ 5,6 à 7,3 kbar et 750 à 810 °C. L'ensemble de wacke et de mudstone semble être lié au groupe Burntwood du Domaine de Kiseynew et s'est probablement déposé relativement à proximité du collage d'arcs de Flin Flon. Le gneiss à hornblende et le silicate calcique sont interprétés comme étant des roches mafiques altérées de manière variable, possiblement des basaltes, et peuvent être liés au magmatisme d'arcs successeurs de la période mississippienne. Selon un modèle proposé, l'eau de ruissellement oxygénée drainant le collage d'arcs de Flin Flon était enrichie de vanadium. L'eau de ruissellement était déversée dans le bassin anoxique de Kiseynew, où les ions de vanadium V^{5+} relativement mobiles ont été réduits à la forme V^{4+} moins mobile, puis absorbée par la matière organique. La décantation des particules organiques en eau de fond possiblement euxinique a réduit encore plus le vanadium en une forme V^{3+} relativement immobile. Après l'enfouissement et le métamorphisme, les dépôts riches en matière organique se sont transformés en horizons graphitiques enrichis de vanadium dans l'ensemble de wacke et de mudstone. Selon le modèle, le vanadium serait fractionné de l'eau peu après la décharge dans le bassin anoxique de Kiseynew, et ces horizons graphitiques à une certaine proximité du collage d'arcs de Flin Flon présentent un potentiel d'enrichissement en vanadium plus important.

TABLE OF CONTENTS

	Page
Abstract / Résumé	iii
Introduction.....	1
Regional geology	2
Kisseynew domain	2
Burntwood group	3
Missi group.....	3
Structure and metamorphism	3
Sub-Phanerozoic Kisseynew domain	4
Thompson nickel belt.....	4
Ospwagan group.....	4
Geology of the Huzyk Creek area	4
Hornblende gneiss and calcsilicate	5
Wacke-mudstone	5
Intrusions	6
Chloritized and hematized gneiss	8
Lithogeochemistry and Sm-Nd isotope geochemistry.....	8
Sampling and analytical methods	9
Hornblende gneiss and calcsilicate	11
Wacke-mudstone	12
Intrusions	14
Chloritized and hematized gneiss	15
Metamorphism.....	15
Methods.....	15
Mineral assemblages	15
Phase equilibrium modelling	16
Discussion.....	18
Intrusions and chloritized and hematized gneiss	18
Stratigraphic affinity of the wacke-mudstone sequence.....	19
Affinity of the hornblende gneiss and calcsilicate.....	22
Depositional model and economic considerations	22
Acknowledgments.....	26
References.....	26

TABLES

Table 1: Summary of lithogeochemical results for representative rock samples from the Huzyk Creek property.....	10
Table 2: Summary of Sm-Nd isotopic data for select rock samples from the Huzyk Creek property	11

FIGURES

Figure 1: Geological domains along the Superior boundary zone, central Manitoba	1
Figure 2: Tectonic-elements map of the Manitoba–Saskatchewan segment of the Trans-Hudson orogen	2
Figure 3: Schematic logs of drillcores HZ-19-1 and HZ-19-2 from the Huzyk Creek property	5
Figure 4: Drillcore images of hornblende gneiss and calcsilicate	6
Figure 5: Drillcore images of the wacke-mudstone suite	7

Figure 6: Drillcore and thin section images of intrusive rocks	8
Figure 7: Drillcore and thin section images of chloritized and hematized rocks from drillhole HZ-19-2	9
Figure 8: Geochemical diagrams for the hornblende gneiss and calcsilicate	12
Figure 9: Discrimination diagrams for rocks of the Huzyk Creek property	13
Figure 10: Multi-element profiles of wacke-mudstones normalized to average P2 pelite	14
Figure 11: Chondrite-normalized rare-earth element profiles and primitive mantle-normalized multi-element profiles for tonalite and metasomatized granite from Huzyk Creek	15
Figure 12: Multi-element diagrams of the chloritized and hematized gneiss normalized to primitive mantle and average P2 pelite	16
Figure 13: Photomicrographs of hornblende gneiss and wacke-mudstone samples	17
Figure 14: Phase diagram sections in NCKFMASHT	18
Figure 15: Primitive mantle-normalized multi-element diagrams for metasomatized rocks from the Burntwood igneous complex, the Brezden Lake igneous complex, and the Eden Lake igneous complex.....	19
Figure 16: Multi-element diagrams of the chloritized and hematized gneiss	20
Figure 17: Multi-element diagrams of Thompson nickel belt and Kisseynew domain semipelitic to pelitic rocks, normalized to average P2 pelite.....	21
Figure 18: Initial ϵ_{Nd} values for Thompson nickel belt, Kisseynew domain, and Huzyk Creek rocks calculated at 1900 Ma.....	22
Figure 19: N-MORB-normalized multi-element diagrams of the Huzyk Creek mafic rocks and geochemically similar mafic rocks from the Flin Flon domain.....	23
Figure 20: Discrimination diagrams comparing the Huzyk Creek mafic rocks with geochemically similar mafic rocks from the Flin Flon domain	24
Figure 21: $V-Al_2O_3^N$ diagram of basalt-paleosol pairs collected in the Flin Flon area.....	25
Figure 22: Schematic model for V-enrichment process in the Kisseynew basin.....	25

APPENDICES

Appendix 1: Core logs and photos for HZ-19-1 and HZ-19-2	GP2020-1.zip
Appendix 2: Whole-rock lithogeochemistry and Sm-Nd isotope geochemistry for samples from the Huzyk Creek property, central Manitoba, and the Flin Flon paleosol, west-central Manitoba (NTS 63J6, 63K13)	GP2020-1.zip
Appendix 3: Thin section point count results for select samples from the Huzyk Creek property.....	GP2020-1.zip

Introduction

The Huzyk Creek property consists of two mineral exploration licenses and 10 mining claims, centred roughly 23 km south of Ponton. The property lies along the boundary between the sub-Phanerozoic Thompson nickel belt (TNB) and Kisseynew domain (Figure 1). A thick (~62 m) interval of sulphide-bearing, graphitic metasedimentary rocks was intersected in diamond-drill core by Hudson Bay Exploration and Development Co. Ltd. while exploring for Ni-Cu on the property in 1997 (Assessment File 73152, Manitoba Agriculture and Resource Development, Winnipeg). The graphitic interval was found to contain up to 40% graphite as fine to coarse flakes. Rocas del Norte, a private company, resampled a 68 m graphitic interval from drillhole NIM-19 in 2014, which yielded 0.14% V_2O_5 , including 0.6% V_2O_5 over 0.6 m (Beaumont-Smith, 2018; Assessment File 73152). The property was optioned by Vanadian Energy Corp. (Vanadian; formerly Uracon) in August of 2018. Recent diamond-drilling by Vanadian attempted to twin NIM-19 as well as test a

geophysical conductor, outlined by historical exploration work, believed to coincide with the graphitic horizon. Attempts to twin hole NIM-19 were not successful due to uncertainty of the original location of the drill collar; however, the first drill-hole, HZ-19-01, intersected a 13.77 m sulphide-bearing graphitic zone grading 0.18% V_2O_5 , including a 9.74 m zone grading 0.22% V_2O_5 (Vanadian Energy Corporation, 2019). The second hole, HZ-19-02, was collared 200 m northeast along strike and intersected a 14.05 m graphitic zone grading 0.11% V_2O_5 . Both graphitic horizons are hosted in metasedimentary rocks with broad zones of variable graphite content and anomalous vanadium (Vanadian Energy Corporation, 2019).

Both graphite and vanadium are considered critical minerals/elements by the U.S. Department of the Interior (United States Geological Survey, 2017). Some of the many uses of graphite include refractory applications, brake linings, motor brushes, and steel making; however, higher valued coarse-grained graphite is used in high-temperature lubricants, and

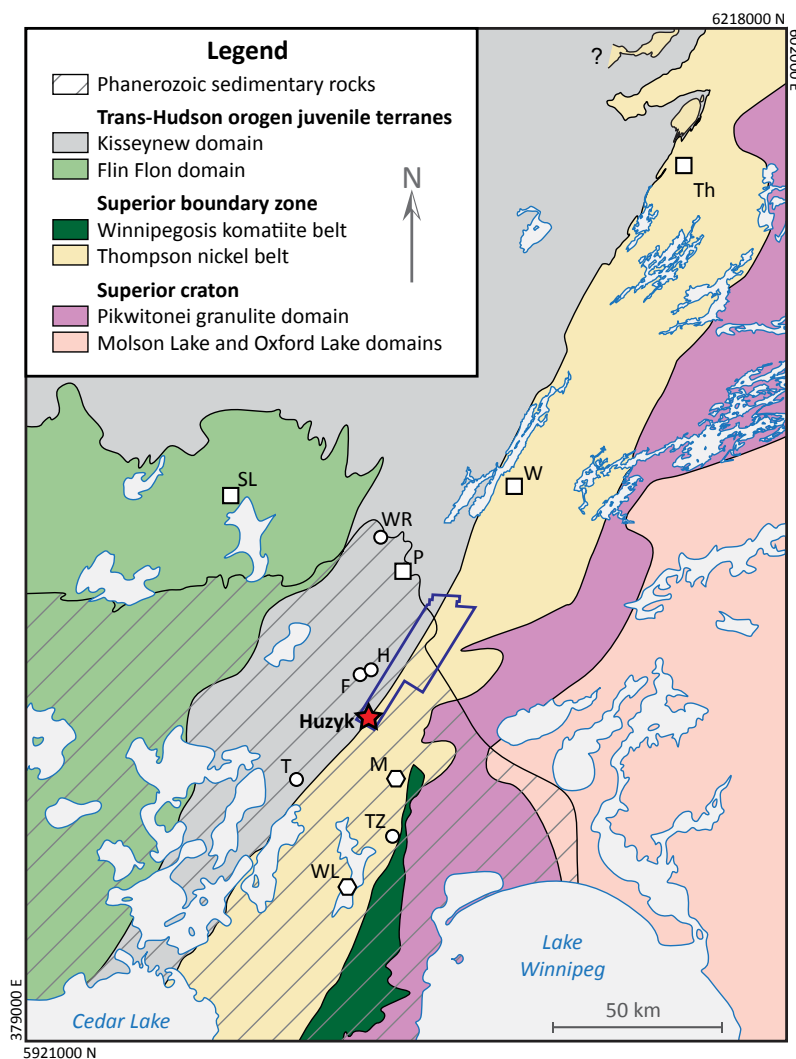


Figure 1: Geological domains along the Superior boundary zone, central Manitoba (modified from Couëslan, 2018a). The dark blue outline is the approximate location of Vanadian's Huzyk Creek property. Symbols: circles, Cu-Zn deposits in the sub-Phanerozoic Kisseynew domain and Superior boundary zone; hexagons, Ni-Cu deposits/occurrences in the sub-Phanerozoic Thompson nickel belt; squares, town/cities; star, location of the 2019 diamond-drilling campaign at the Huzyk Creek property. Abbreviations: F, Fenton deposit; H, Harmin deposit; M, Minago deposit; P, Ponton; SL, Snow Lake; T, Talbot deposit; Th, Thompson; TZ, Tower zone deposit; W, Wabowden; WL, William Lake occurrence; WR, Watts River deposit. Co-ordinates are in UTM Zone 14, NAD83.

lithium battery and fuel cell applications (Robinson et al., 2017). Vanadium is used primarily in the production of high-strength steels, and specialty aluminum and titanium alloys. In the field of green technology there is growing interest around the use of vanadium redox-flow batteries for large-scale energy storage (Kelley et al., 2017). These batteries boast the potential for nearly unlimited storage capacity and unlimited lifespan.

Sulphide- and graphite-bearing argillaceous rocks occur in both the Burntwood group rocks of the Kisseynew domain and Ospwagan group rocks of the TNB (Zwanzig, 1999; Zwanzig et al., 2007; Callinex Mines Incorporated, 2014; Martins and Couëslan, 2019). Because the Huzyk Creek property straddles the TNB–Kisseynew domain boundary, determining the affinity of the metasedimentary rocks has implications for locating additional vanadium-bearing graphitic horizons. The objectives of this project are to evaluate the rocks hosting the graphite and vanadium mineralization at Vanadian’s Huzyk Creek property and determine their affinity to either the TNB or Kisseynew domain, and to derive possible petrogenetic model(s) for the mineralization.

Regional geology

Kisseynew domain

The Huzyk Creek property lies along the sub-Phanerozoic boundary between the Kisseynew domain and the TNB.

The Kisseynew domain is situated in the core of the juvenile Reindeer zone of the Paleoproterozoic Trans-Hudson orogen (THO; Figure 2). It is underlain by dominantly Burntwood group rocks, with subordinate calcalkaline plutons and sheets of anatectic granitoids. The Burntwood group forms a monotonous sequence of graphite-bearing metagreywacke-mudstone, which was metamorphosed to garnet-biotite gneiss and migmatite throughout much of the Kisseynew domain during the terminal collision of the THO. The metagreywacke-mudstone is interpreted as turbidite deposits shed from the surrounding juvenile accretionary-arc complexes of the Flin Flon and Lynn Lake domains (Ansdell et al., 1995; Zwanzig and Bailes, 2010). Coeval fluvial-alluvial deposits on the margins of these volcano-plutonic domains consist of the Missi and Sickie groups, respectively (Stauffer, 1990; Zwanzig and Bailes, 2010). The Kisseynew paleobasin is generally interpreted as a back-arc basin; however, an inter-arc or fore-arc basin environment could also be possible (Ansdell et al., 1995; Zwanzig, 1997; Corrigan et al., 2009; Zwanzig and Bailes, 2010).

The Kisseynew domain of Manitoba has been divided into four subdomains: the central Kisseynew subdomain, Kisseynew north flank, Kisseynew south flank, and the north-east Kisseynew subdomain (Figure 2; Zwanzig and Bailes, 2010). The central subdomain consists dominantly of Burntwood group rocks with subordinate calcalkaline plutons and sheets of anatectic granitoids. The north flank borders the

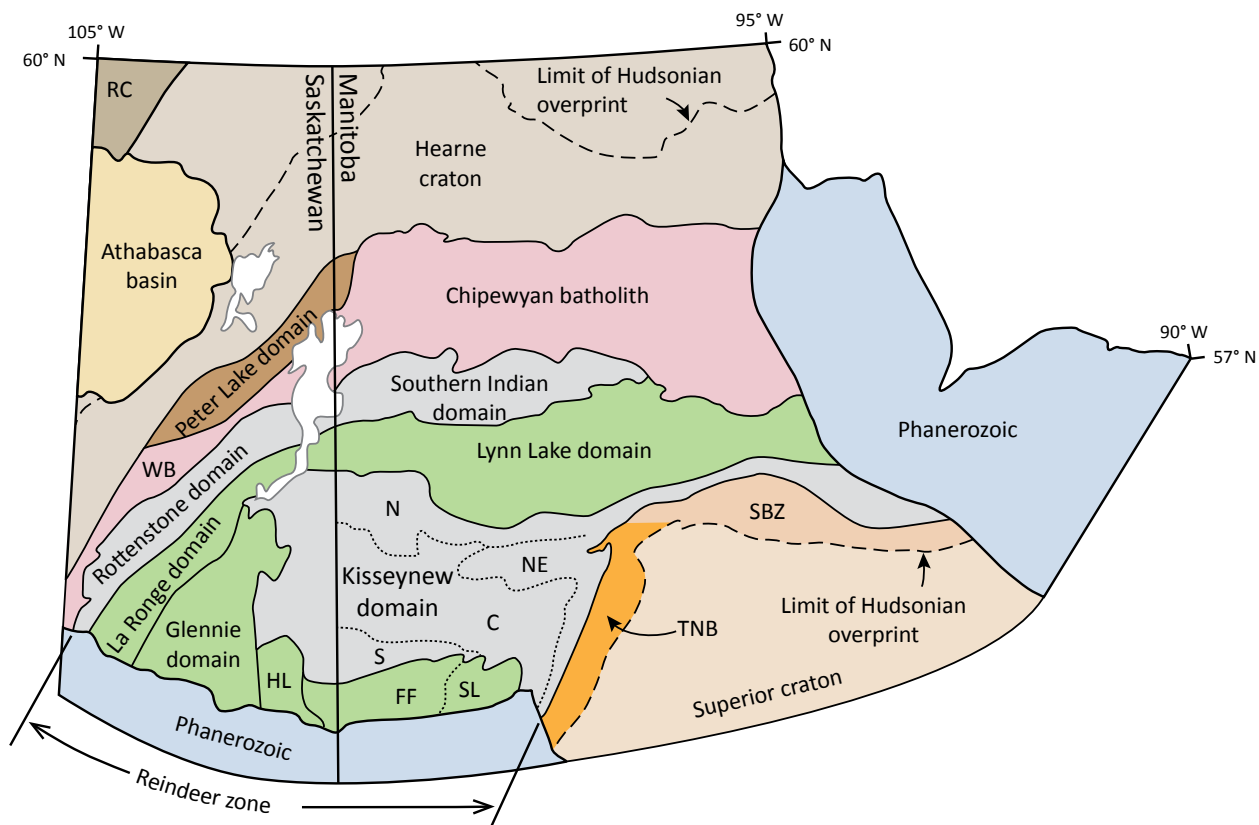


Figure 2: Tectonic-elements map of the Manitoba–Saskatchewan segment of the Trans-Hudson orogen (modified from Lewry et al., 1990). Abbreviations: C, central Kisseynew subdomain; FF, Flin Flon domain; HL, Hanson Lake block; N, Kisseynew north flank; NE, northeastern Kisseynew subdomain; RC, Rae craton; S, Kisseynew south flank; SBZ, Superior boundary zone; SL, Snow Lake subdomain; TNB, Thompson nickel belt; WB, Wathaman batholith.

adjacent Lynn Lake domain and consists of structurally inter-layered gneissic units derived from the Burntwood and Sickle groups, and back-arc–basin basalt and plume-related volcanic rocks. The south flank borders the Flin Flon domain and consists of structurally interlayered Burntwood and Missi group rocks. The northeastern subdomain borders the TNB and consists of Burntwood group and subordinate plutons, structurally interleaved with Grass River group and Archean gneiss.

Burntwood group

The Burntwood group consists of a sequence of turbidite-derived greywacke-mudstone deposits. Over most of the Kiseynew domain these rocks occur as migmatitic garnet-biotite gneiss commonly with sillimanite and cordierite, and minor graphite. Locally preserved rhythmic layering alternates between more quartzofeldspathic gneiss and more biotite- and garnet-rich gneiss, and is interpreted as graded greywacke-mudstone beds. Local pods of calcsilicate are probably derived from calcareous concretions (Corrigan and Rayner, 2002; Zwanzig et al., 2007). The Burntwood group grades laterally and vertically into the fluvial-alluvial successions of the Missi, Sickle, and Grass River groups. Narrow packages containing sporadic hornblende, magnetite, or pyrrhotite are interpreted as part of the Burntwood group–Grass River group transition (Zwanzig et al., 2007). Similar transitional deposits exist with the Missi and Sickle groups.

Deposition of the Burntwood group likely began around ca. 1865 Ma as distal turbidites in prograding submarine fans along the margin of the Flin Flon domain (Ansdell et al., 1995; Machado et al., 1999; Zwanzig and Bailes, 2010). These deposits may have preceded that of the Missi group until ca. 1848 Ma, when deposition became synchronous. The youngest detrital zircons analyzed from the Burntwood group yielded ages of ca. 1845–1841 Ma (Machado et al., 1999), and a minimum age for deposition is provided by the ca. 1830–1820 Ma Touchbourne suite, which intrudes the Burntwood group rocks (Gordon et al., 1990; Machado et al., 1999; Zwanzig and Bailes, 2010).

Missi group

The Missi group consists of fluvial-alluvial sandstones and conglomerate that unconformably overlie the Amisk collage and successor-arc plutons of the Flin Flon domain (Stauffer, 1990; Zwanzig, 1999). Deposition likely occurred in isolated fault-bounded sub-basins that drained into the Kiseynew basin (Zwanzig and Bailes, 2010). Subordinate, mafic to felsic volcanic rocks occur throughout the succession (Gordon and Lemkow, 1987; Machado et al., 1999). A paleoregolith can occur as far as 10 m below the unconformity, indicating subaerial weathering for a significant period of time, possibly on the order of several million years (Stauffer, 1990). A considerable amount of hematite and/or magnetite is present in the Missi group (approximately 3% overall, locally >30%), and qualifies these rocks as redbed deposits (Stauffer, 1990; Zwanzig, 1999).

The deposits are largely coeval with the Burntwood group, and are correlative with the fluvial-alluvial Sickle and Grass River groups of the Lynn Lake domain and western margin of the TNB, respectively.

The basal conglomerate of the Missi group is intruded by a ca. 1848 Ma dacite (Machado et al., 1999), and felsic volcanic rocks in the upper part of the Missi group are dated at ca. 1832 Ma (Gordon et al., 1990; David et al., 1996). This suggests at least 16 million years of sedimentation, with substantial overlap in the timing of Burntwood group deposition. However, deposition was likely diachronous across the sub-basins. The Missi group prograded over the Burntwood group as the Kiseynew basin was in-filled.

Structure and metamorphism

The rocks of the Kiseynew domain were subject to multiple phases of deformation beginning with a ca. 1845–1825 Ma fold-and-thrust system (D_1/F_1), which likely resulted from the Sask craton under-riding the Flin Flon and Kiseynew domains (Zwanzig, 1999). Thrusting was likely coeval with deposition of the Missi and upper Burntwood groups and directed toward the Kiseynew basin, which would be consistent with the direction of sedimentary transport and the inferred direction of subduction polarity (Machado et al., 1999; Zwanzig, 1999; Zwanzig and Bailes, 2010). However, vergence has also been interpreted as toward the Flin Flon domain, based on the present-day orientation of these structures (Ansdell et al., 1995). D_1 was followed by two generations (F_2 and F_3) of recumbent folding accompanied by prograde metamorphism and the development of a penetrative S_2 – S_3 foliation (Ansdell et al., 1995; Zwanzig, 1999). Westward overturning of D_1 structures during F_2 was a product of east-west compression during collision between the Superior craton and the Flin Flon and Kiseynew domains beginning ca. 1.83–1.82 Ga (Ansdell et al., 1995; Machado et al., 1999; Zwanzig, 1999; Zwanzig and Bailes, 2010). South- and southwest-verging F_3 folding amplified and overturned F_1 – F_2 folds. Much of D_3 is interpreted to coincide with peak metamorphic conditions from ca. 1810 to 1800 Ma (Zwanzig, 1999). Late F_3 folding likely continued until ca. 1789 Ma, and resulted from rocks of the Lynn Lake belt attempting to over-ride the Kiseynew domain, as the Hearne craton attempted to over-ride the Reindeer zone (Zwanzig, 1999). A continuous progression may have occurred between the D_2 and D_3 phases of deformation. In the main portion of the Kiseynew domain, F_4 folds are generally upright and open, with north or east-northeast trends (Zwanzig, 1999). Folding may be accompanied by a retrograde S_4 foliation in hinge zones and lower amphibolite- to greenschist-facies assemblages. Adjacent to the TNB, F_4 folds become tighter, with northeast-trending fold axes, consistent with sinistral transpression along the north-northeast-trending Superior boundary zone (Zwanzig, 1998; Zwanzig, 1999).

The metamorphic grade increases from the flanks of the Kiseynew domain toward the central subdomain (Bailes and McRitchie, 1978; Gordon, 1989; Couëslan and Pattison, 2012). Schists with mineral assemblages of greenschist to lower-amphibolite facies (chlorite–muscovite–garnet) proximal to the north and south flanks of the domain, grade into granulite-facies migmatites (cordierite–garnet–melt/K-feldspar) in the core (Bailes and McRitchie, 1978). Peak metamorphic conditions in the high-grade core are believed to be relatively uniform and estimated at $750 \pm 50^\circ\text{C}$ and 5.5 ± 1 kbar (Gordon, 1989); however, Growdon (2010) suggested grades as high as 900°C and 12 kbar in the central Kiseynew domain. Prograde to peak metamorphism was likely ongoing during D_2 – D_3 from ca. 1820 to 1800 Ma, with peak conditions likely attained at ca. 1810–1800 Ma (Ansdell et al., 1995; Machado et al., 1999; Zwanzig, 1999; Growdon, 2010).

Sub-Phanerozoic Kiseynew domain

The sub-Phanerozoic Kiseynew domain is the southern extension of the Kiseynew domain below the Phanerozoic cover (Figure 1). Situated between the Superior craton margin and the Flin Flon domain, it was interpreted to consist of migmatitic metasedimentary rocks of the Burntwood group interlayered with felsic metaplutonic veins and sheets (Leclair et al., 1997). However, the discovery of several volcanogenic massive sulphide (VMS) deposits (Watts River, Harmin, Fenton, and Talbot) in the domain has brought this interpretation into question (Simard et al., 2010). Recent studies (Simard et al., 2010; Bailes, 2015; Reid, 2018) suggest complex structural interleaving of Flin Flon domain arc rocks, Kiseynew domain Burntwood group rocks, and possibly TNB rocks within the sub-Phanerozoic Kiseynew domain. A similar situation occurs along the north, south, and east flanks of the exposed Kiseynew domain, where thrusts and recumbent folding have structurally interleaved rocks of the Kiseynew basin with rocks of adjacent juvenile volcano-plutonic terranes and evolved Archean crust (Zwanzig, 1999; Rayner and Percival, 2007; Zwanzig and Bailes, 2010).

Thompson nickel belt

The TNB forms a segment of the Superior boundary zone, flanked to the northwest by the Kiseynew domain of the Trans-Hudson orogen and to the southeast by the Pikwitonei granulite domain of the Superior craton (Figure 1). The TNB is underlain largely by reworked Archean gneiss of the Pikwitonei domain (Hubregtse, 1980; Mezger et al., 1990; Heaman et al., 2011), which was exhumed and unconformably overlain by the Paleoproterozoic supracrustal rocks of the Ospwagan group (Bleeker, 1990; Zwanzig et al., 2007). The Archean basement gneiss and Ospwagan group were subjected to multiple generations of deformation and metamorphic conditions, ranging from middle-amphibolite facies to lower-granulite facies, during the Trans-Hudson orogeny (Bleeker, 1990; Burnham et al., 2009; Couëslan and Pattison, 2012).

The dominant phase of penetrative deformation is D_2 , which affected the Ospwagan group and Archean gneiss. This deformation phase resulted in the formation of F_2 nappe structures, which are interpreted as either east verging (Bleeker, 1990; White et al., 2002) or southwest verging (Zwanzig et al., 2007; Burnham et al., 2009). The recumbent folds are associated with regionally penetrative S_2 fabrics. The D_2 phase of deformation is interpreted to be the result of convergence between the Superior craton margin and the Reindeer zone of the Trans-Hudson orogen from ca. 1830 to 1800 Ma. The D_3 phase of deformation resulted in isoclinal folds with vertical to steeply southeast-dipping axial planes (Bleeker, 1990; Burnham et al., 2009). Mylonite zones with subvertical stretching lineations parallel many of the regional F_3 folds. Tightening of D_3 structures continued during D_4 , marked by localized retrograde greenschist-facies metamorphism along northeast-striking, mylonitic and cataclastic shear zones that commonly record southeast-side-up sinistral movement (Bleeker, 1990; Burnham et al., 2009).

Ospwagan group

The following summary of the Ospwagan group is sourced largely from Bleeker (1990) and Zwanzig et al. (2007). The Paleoproterozoic Ospwagan group unconformably overlies Archean basement gneiss in the TNB. The lowermost unit of the Ospwagan group is the Manasan formation, a fining-upward transgressive sequence of sandstones and semipelitic rocks. This grades into the overlying Thompson formation, a succession of calcsilicates and impure marbles that reflects a transition to a carbonate-dominated system. The Thompson formation is overlain by the Pipe formation, a sequence of deep-water deposits including silicate- and sulphide-facies iron formations, cherts, mudstones, calcsilicates, and marble. Overlying this is the Setting formation, a coarsening-upward succession of interbedded sandstones and mudstones that were likely deposited as turbidites. The Ospwagan group is capped by the Bah Lake assemblage, which consists of mafic to ultramafic volcanic rocks dominated by massive to pillowed basalt flows with local picrite and minor synvolcanic intrusions.

Geology of the Huzyk Creek area

Core from drillholes HZ-19-1 and HZ-19-2 was logged in August of 2019. The order of the rock units is described from the structural hangingwall of the graphite- and vanadium-enriched zone into the footwall (Figure 3). All the rocks described attained relatively high metamorphic grade during the Trans-Hudson orogeny. Protolith interpretation was used for naming rocks where a fair amount of certainty exists; however, where ambiguity remains, metamorphic nomenclature was retained. The ‘meta-’ prefix has been omitted from rock names for brevity. All rocks have a well-developed penetrative foliation with the exception of some granite intrusions that are weakly foliated. Reported thicknesses are intersection lengths, not true

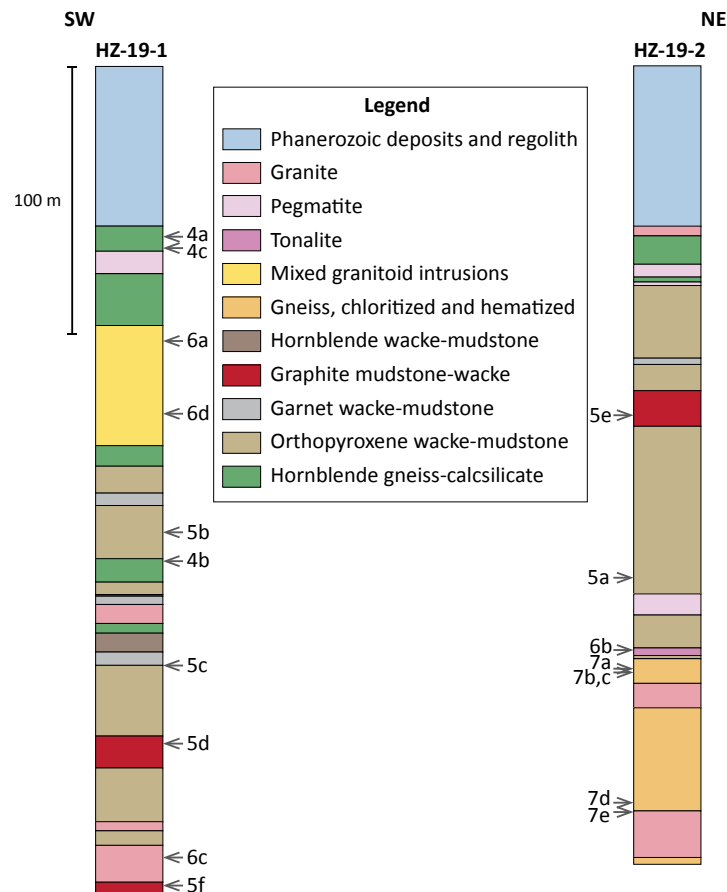


Figure 3: Schematic logs of drillcores HZ-19-1 and HZ-19-2 from the Huzyk Creek property; see Figure 1 for the approximate location. The stratigraphic position of images in Figures 4 to 7 are indicated along the inside edge of each column.

thicknesses. Drill logs and accompanying photos can be found in Appendix 1.

Hornblende gneiss and calcsilicate

Intervals of interlayered hornblende gneiss and calcsilicate occur at the top of the Precambrian in both drillholes. The hornblende gneiss is medium grained and plagioclase rich, with 30–40% hornblende. Less than 20% orthopyroxene + clinopyroxene can be intergrown with the hornblende. The gneiss locally grades into amphibolite, which contains 50–60% hornblende. The gneiss and amphibolite locally contain garnet porphyroblasts <7 mm across that are characterized by plagioclase corona. More common are rounded aggregates of plagioclase <8 mm across that are likely pseudomorphous after garnet (Figure 4a). In general, the calcsilicate is texturally similar to the hornblende gneiss, with the hornblende replaced by pale green clinopyroxene and the addition of sparse titanite. The calcsilicate and hornblende gneiss can be interlayered on scales ranging from <1 cm to 2.5 m, with diffuse contacts (Figure 4b). In drillhole HZ-19-1 the hornblende gneiss and calcsilicate are interleaved with the underlying wacke at a scale of <35 m. A possible second variety of calcsilicate is also present in drillhole HZ-19-1. It is a coarse-grained rock with variable enrichment in diopside, sulphide, titanite and epidote. Rather than being interlayered with the hornblende gneiss, it occurs

as diffuse bands that locally appear to cross-cut the regional fabrics (Figure 4c). The cross-cutting relationship suggests that the coarse-grained calcsilicate may be derived from a later metasomatic event.

Wacke-mudstone

The graphite- and vanadium-enriched horizon is hosted by a thick package of interbedded migmatitic wackes and mudstones. The various wackes and mudstones are named for the dominant mafic mineral, exclusive of biotite, that is present in the rock. The wackes appear as medium- to coarse-grained quartzofeldspathic gneisses, typically with 10–20% biotite. The compositionally similar mudstones are medium to coarse grained, schistose, and arbitrarily defined as having >20% biotite (typically 20–30%). The wacke-mudstone units are described in order of decreasing abundance.

Orthopyroxene wacke is the most abundant lithology in this package. It typically contains 7–10% orthopyroxene, which locally forms coarse-grained poikiloblasts <1 cm across (Figure 5a). Garnet is common, but typically makes up less than 3% of the rock. Local horizons contain trace amounts of graphite and <3% pyrrhotite. The wacke is locally interbedded with orthopyroxene mudstone layers <2 m thick (Figure 5b). Local layers in the mudstone can contain trace amounts of graphite, and sparse garnet and pyrrhotite. Orthopyroxene in both the

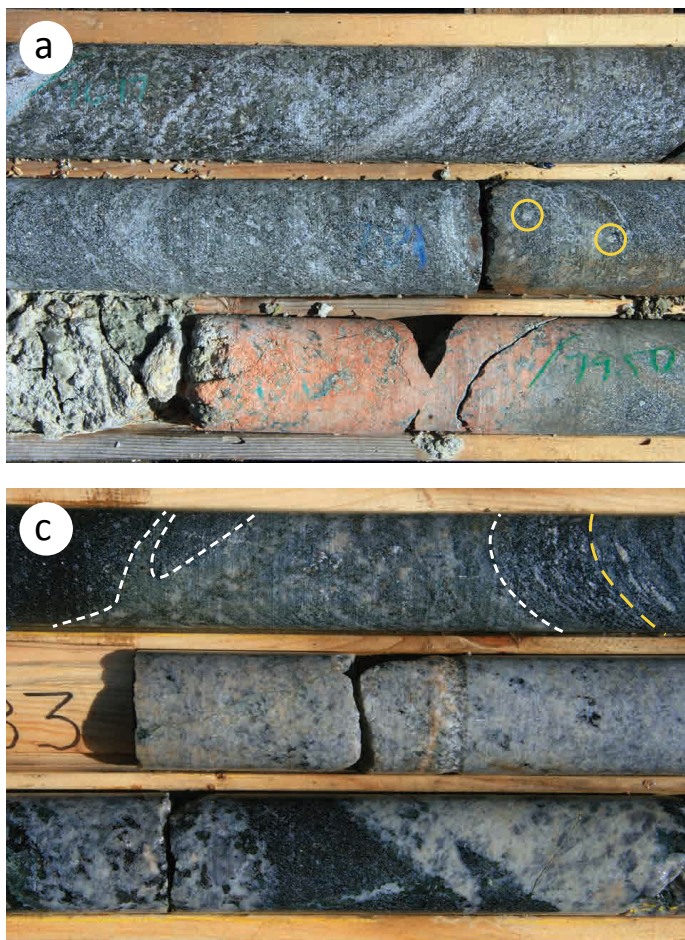


Figure 4: Drillcore images of hornblende gneiss and calcsilicate: **a)** hornblende gneiss grading into plagioclase amphibolite (top two rows), circles indicate plagioclase pseudomorphs after garnet (HZ-19-1, 76.4 m); **b)** calcsilicate interlayered with hornblende gneiss (top two rows), circles indicate garnet porphyroblasts (HZ-19-1, 221.65 m); **c)** discordant zone of calcsilicate (top row, outline in white) hosted in hornblende gneiss (the trace of the regional rock fabric/layering is outlined in yellow), the hornblende gneiss is intruded by pegmatitic granite that is locally hornblende- and titanite-bearing (bottom row; HZ-19-1, 81.55 m). Drillcore is NQ with a diameter of 47.5 mm.

wacke and mudstone can be pseudomorphously replaced by cummingtonite.

The orthopyroxene wacke-mudstone hosts local layers of garnet wacke-mudstone <6 m thick (Figure 5c). In addition to biotite, the garnet wacke contains 3–5% orthopyroxene and 5–7% garnet. Garnet and orthopyroxene typically occur along diffuse, alternating layers, likely controlled by primary compositional bedding of the sedimentary rock. Trace amounts of graphite and pyrrhotite are typically present, but up to 3% graphite and pyrrhotite can occur. The garnet wacke is locally interlayered with garnet mudstone beds <30 cm thick; in addition, the garnet mudstone can occur as layers <3 m thick within the orthopyroxene wacke-mudstone unit. The garnet mudstone typically contains trace to 2% graphite and 5–20% garnet. Orthopyroxene typically forms <5% of the rock, although the garnet mudstone and orthopyroxene mudstone can be interlayered on a scale of <1 cm.

Graphite mudstone occurs as a discrete horizon, 14.3–16.7 m wide, within the overall wacke-mudstone sedimentary rock package. The graphite mudstone contains 3–7% pyrrhotite, 10–30% biotite, and 20–30% graphite (Figure 5d). Trace amounts of chalcopryite, molybdenite and sphalerite are typically present. The mudstone contains local beds of pyrrhotite-graphite wacke (Figure 5e) <1.8 m thick. The pyrrhotite-graphite wacke is typically fine to medium grained and

contains 1–3% graphite, 2–5% pyrrhotite, 10–15% biotite, and sparse orthopyroxene. A second discrete horizon of graphitic wacke, at least 5.2 m thick, occurs at the bottom of drillhole HZ-19-1. This wacke is distinct from the one interbedded with the graphite mudstone in that it appears as graphite-bearing orthopyroxene wacke and garnet wacke interbedded on a scale <1.4 m. The graphite content in these interbedded wackes is typically 2–3% but is locally as high as 5%. Local sillimanite-rich beds <5 cm thick are also present (Figure 5f).

A single hornblende wacke-mudstone layer (8.45 m thick) occurs within the core of drillhole HZ-19-1. The hornblende wacke contains 5–7% hornblende, 5–7% orthopyroxene, and 2–3% clinopyroxene. A thin section reveals the hornblende to be intergrown with cummingtonite, and that the amphibole intergrowths are likely pseudomorphous after orthopyroxene and clinopyroxene. The mudstone occurs as beds <30 cm thick within the wacke. The sequence is in direct contact with an interval of calcsilicate and hornblende gneiss. The hornblende wacke-mudstone could represent a more calcareous section, or an influx of volcanoclastic detritus.

Intrusions

Several varieties of granitoid rocks are present in the drillcore (Figure 6a). The intrusions appear to intersect all of the previously described units. Local intersections of coarse-

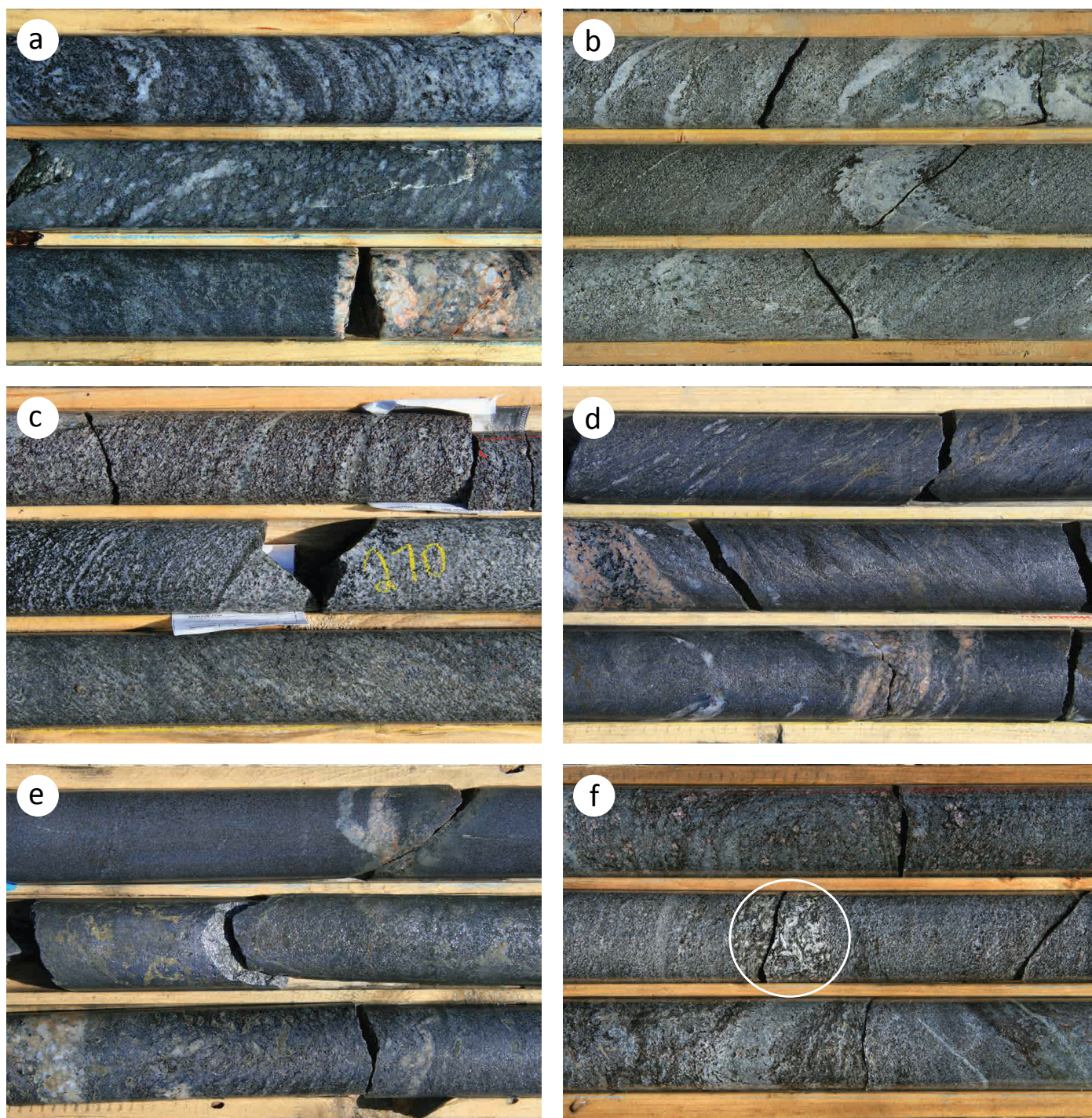


Figure 5: Drillcore images of the wacke-mudstone suite: **a)** orthopyroxene wacke with coarse-grained orthopyroxene poikiloblasts (middle row; HZ-19-2, 239.7 m); **b)** orthopyroxene wacke (top and bottom rows) interbedded with orthopyroxene mudstone (middle row; HZ-19-1, 208.6 m); **c)** garnet wacke (top row) interbedded with orthopyroxene wacke (bottom row; HZ-19-1, 268.5 m); **d)** graphite mudstone (HZ-19-1, 303.2 m); **e)** graphite-pyrrhotite wacke (top row) hosted in graphite mudstone (bottom two rows; HZ-19-2, 163.65 m); **f)** graphitic garnet wacke (top row) and graphitic orthopyroxene wacke (bottom two rows) with local sillimanite-rich beds (circled; HZ-19-1, 367.1 m). Drillcore is NQ with a diameter of 47.5 mm.

grained tonalite <3.5 m occur in both drillholes (Figure 6a, b). The tonalite is light grey and typically contains 3–7% biotite and 3–7% hornblende, along with variable but minor amounts of orthopyroxene, pyrrhotite and titanite. The tonalite is commonly migmatitic and intruded by pegmatite and medium-grained granite. Sparse intervals of granodiorite <6 m wide

are present in drillhole HZ-19-1. It is pinkish grey and biotite bearing, with minor amounts of amphibole. The granodiorite is intruded by pegmatite and tonalite (Figure 6a). Pink, medium-grained biotite granite occurs as intrusions in both drillholes (Figure 6c). The granite intersections vary from centimetres up to 22 m wide. The rock is pink, weakly foliated to foliated, and

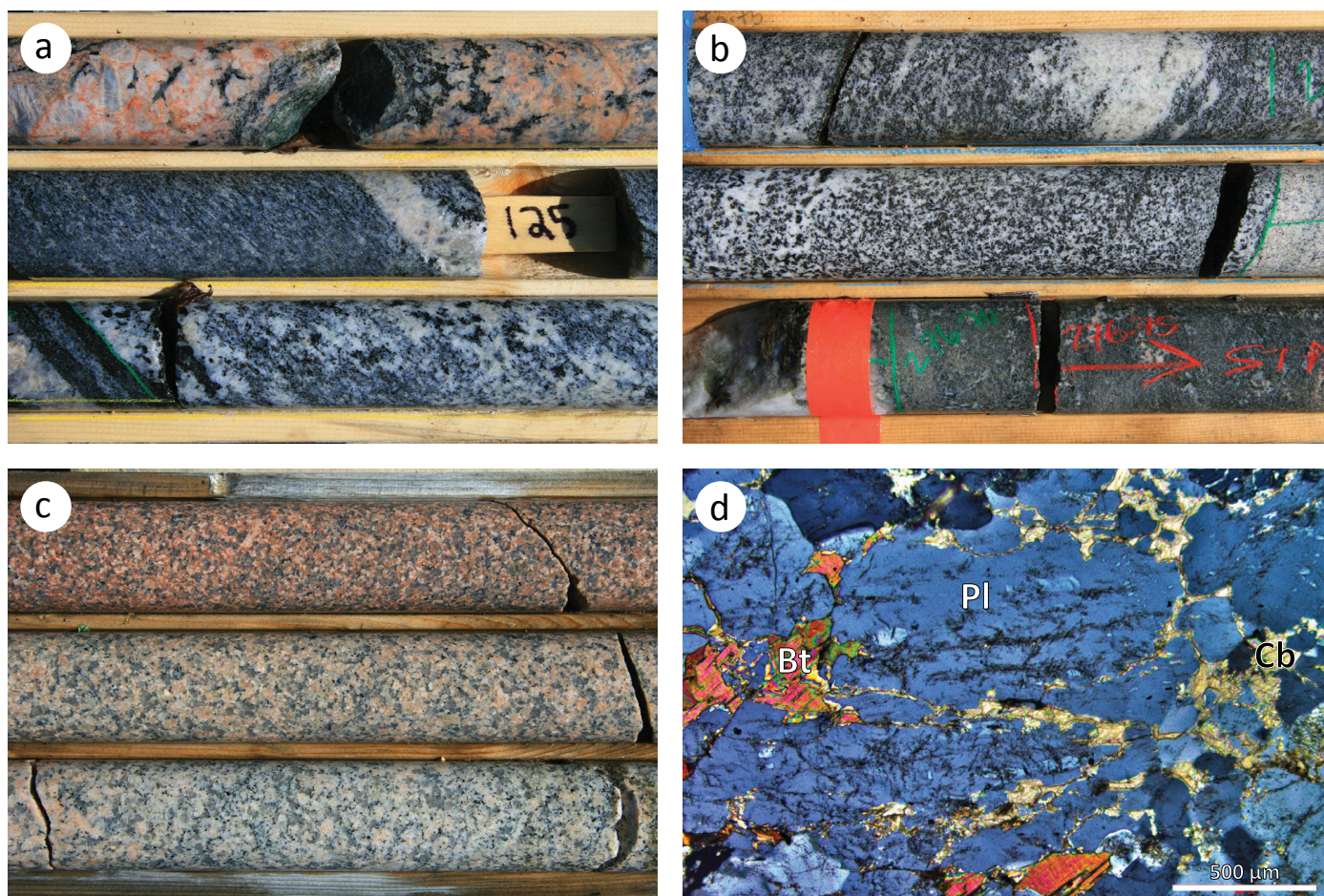


Figure 6: Drillcore and thin section images of intrusive rocks: **a)** granodiorite (middle row) intruded by pegmatitic granite (top row) and tonalite (bottom row; HZ-19-1, 123.3 m); **b)** retrogressed orthopyroxene wacke (bottom row) intruded by tonalite (top two rows; HZ-19-2, 273.75 m); **c)** weakly foliated biotite granite (HZ-19-1, 354.2 m); **d)** photomicrograph in cross-polarized light of carbonate and biotite micro-veinlets cross-cutting antiperthitic plagioclase in metasomatized granite (sample 108-19-HZ22). Drillcore is NQ with a diameter of 47.5 mm. Abbreviations: Bt, biotite; Cb, carbonate; Pl, plagioclase.

relatively even textured, although local pegmatite segregations can be present.

Pegmatitic granite is abundant in the drillcore and forms intersections ranging from centimetres up to 10 m in width. Several generations of pegmatite are likely present. They range from pink to light grey, and are typically biotite bearing (Figure 4a, Figure 6a); however, local intrusions may contain minor hornblende, pyrrhotite, and titanite (Figure 4c). A thin section of titanite- and hornblende-bearing pegmatitic granite revealed micro-veinlets of carbonate and biotite (Figure 6d), the partial replacement of plagioclase and hornblende by biotite and carbonate, and a strong association of titanite and allanite with the biotite and carbonate. Relatively coarse antiperthite is common along with zones of myrmekite. The veinlets, replacement textures, and feldspar exsolution textures suggest the granite was metasomatically overprinted.

Chloritized and hematized gneiss

A 96 m interval of intensely chloritized and hematized gneiss occurs at the bottom of drillhole HZ-19-2. The gneiss is medium to coarse grained and is albite rich, with 7–10% hema-

tite and 10–30% chlorite (Figure 7a). Both specular and earthy hematite are present. Trace amounts of piemontite are visible in thin section (Figure 7b, c). Local zones within the gneiss have a mottled texture (Figure 7d). Sparse zones of quartz-vein breccia <2 m wide can contain void-filling specular hematite. Intrusions of pegmatite and medium-grained granite within this interval are overprinted by the chlorite and hematite alteration (Figure 7e). The protolith of the chloritized and hematized gneiss is uncertain; however, the mafic content is comparable to the wacke-mudstone rocks, and the local mottling could represent the pseudomorphous replacement of poikiloblastic orthopyroxene. A sample was collected for lithogeochemical analysis and comparison with other units.

Lithogeochemistry and Sm-Nd isotope geochemistry

Twenty-two samples, representing most of the major units, were collected for lithogeochemistry. In addition, Sm-Nd isotope geochemistry was obtained for three samples of wacke and one sample of hornblende gneiss. Results of the lithogeochemical and Sm-Nd isotope analyses are provided in Appen-

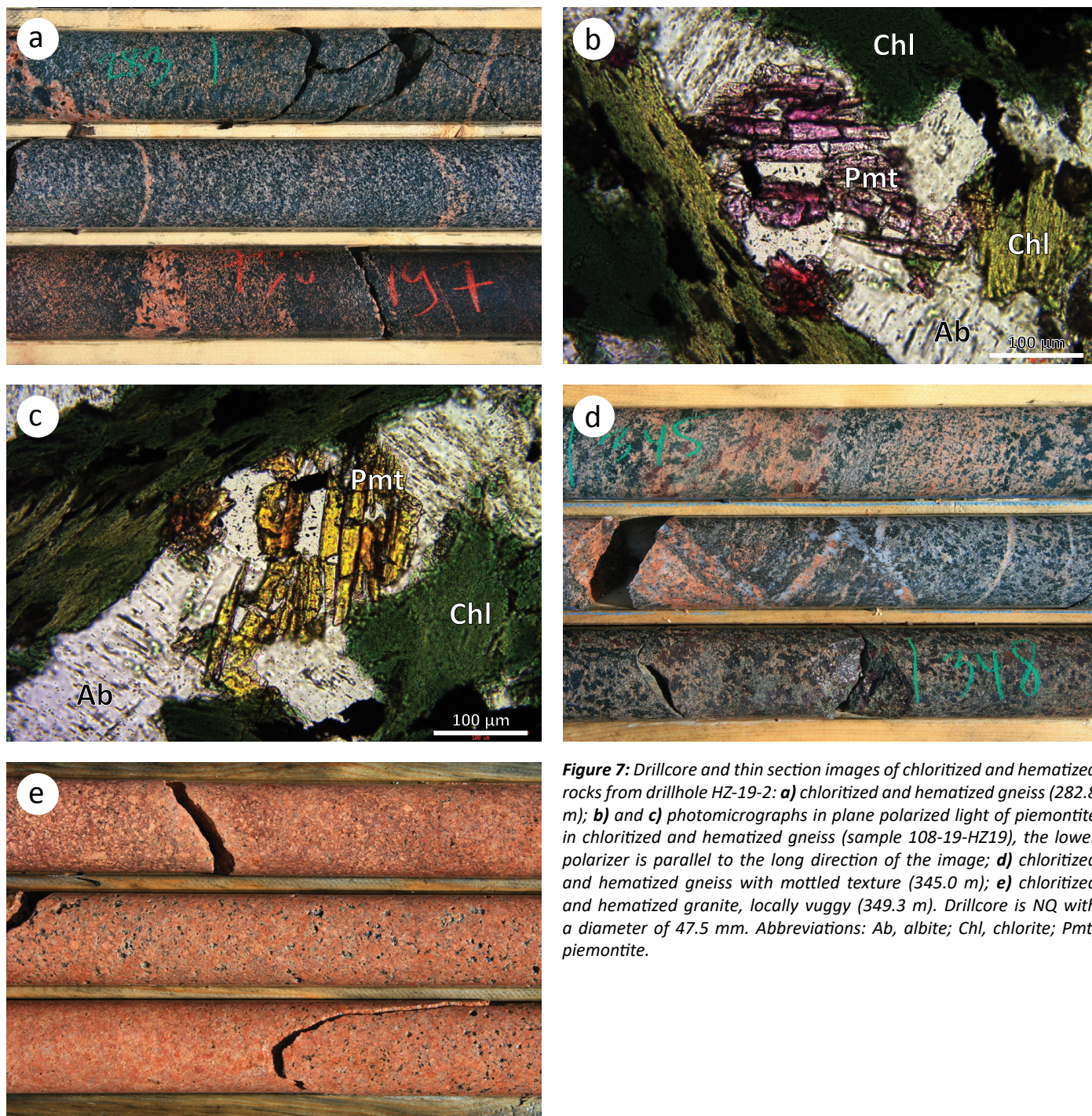


Figure 7: Drillcore and thin section images of chloritized and hematized rocks from drillhole HZ-19-2: **a)** chloritized and hematized gneiss (282.8 m); **b)** and **c)** photomicrographs in plane polarized light of piemontite in chloritized and hematized gneiss (sample 108-19-HZ19), the lower polarizer is parallel to the long direction of the image; **d)** chloritized and hematized gneiss with mottled texture (345.0 m); **e)** chloritized and hematized granite, locally vuggy (349.3 m). Drillcore is NQ with a diameter of 47.5 mm. Abbreviations: Ab, albite; Chl, chlorite; Pmt, piemontite.

dix 2, and representative analyses are summarized in Table 1 and Table 2, respectively.

Sampling and analytical methods

Representative samples were collected from most of the principal units for geochemical analysis. Approximately 30 cm long samples of representative material were selected from the drillcore. The core was sawn length-wise with one half of the core returned to the core box and the other half being retained for geochemical analysis, thin section, and archive. Samples were crushed to <5 mm at the Manitoba Geological Survey Midland Sample and Core Library using a steel jaw-

crusher. Pulps were produced in a steel swing mill and were homogenized by rolling and then splitting to approximately 55 g of analytical material. Two internal standards and two blind duplicates were inserted along with the 22 samples submitted for analysis.

Samples were analyzed at Activation Laboratories Ltd. (Ancaster, Ontario) using the '4Litho' and '4Lithoresearch' analytical packages, which employ a lithium metaborate/tetraborate fusion technique, followed by nitric-acid digestion and analysis by inductively coupled plasma-optical emission spectrometry (ICP-OES) for the major elements and selected trace elements (Ba, Be, Sc, Sr, V, Y, Zr), and inductively coupled

Table 1: Summary of lithogeochemical results for representative rock samples from the Huzyk Creek property.

	Hornblende gneiss		Calc-silicate	Wacke-mudstone								Intrusions		Chl Hem gneiss
Sample	108-19-HZ01	108-19-HZ20	108-19-HZ07	108-19-HZ14	108-19-HZ15	108-19-HZ18	108-19-HZ07	108-19-HZ08	108-19-HZ10	108-19-HZ16	108-19-HZ04	108-19-HZ03	108-19-HZ22	108-19-HZ19
Subunit				Opx wacke	Opx mudstone	Opx wacke	Grt mudstone	Grt wacke	Gr mudstone	Gr mudstone	Hbl wacke	Tonalite	Met granite	
(wt. %)														
SiO ₂	49.85	48.35	50.39	59.25	50.91	62.43	52.21	47.64	39.79	44.2	57.89	58.68	61.95	47.47
Al ₂ O ₃	13.42	14.14	14.49	13.37	18.8	15.14	18.12	18.48	9.62	9.79	15.53	17.21	16.28	17.95
Fe ₂ O ₃	13.91	15.24	9.9	10.85	11.65	7.94	11.51	16.01	12.87	12.09	9.58	7.16	3.04	11.52
MnO	0.201	0.207	0.172	0.112	0.098	0.078	0.093	0.136	0.029	0.037	0.117	0.092	0.047	0.26
MgO	4.75	7.16	4.36	6.86	5.98	4.41	5.68	7.5	1.48	2.43	4.6	2.96	1.18	7.69
CaO	11.02	9.74	13.84	3.41	3.8	4.17	3.4	2.85	1.14	0.25	5.02	5.55	4.17	2.24
Na ₂ O	2.98	3.07	3.02	2.54	3.57	3.63	3.54	2.91	1.65	0.62	3.66	4.01	3.22	4.97
K ₂ O	0.77	0.71	0.55	2.1	2.72	1.64	3.72	2.68	3.81	4.28	1.59	1.78	5.44	1.1
TiO ₂	2.031	1.341	1.828	1.105	1.057	0.739	0.941	1.268	0.402	0.491	0.835	0.919	1.465	1.69
P ₂ O ₅	0.21	0.12	0.21	0.08	0.09	0.09	0.09	0.04	0.16	0.02	0.36	0.38	0.42	0.66
LOI	1.6	0.26	1.63	0.69	0.67	0.34	0.98	0.51	27.37	25.09	1.38	1.14	1.42	4.45
Total	100.7	100.3	100.4	100.4	99.34	100.6	100.3	100	98.32	99.3	100.6	99.88	98.64	100
C	na.	na.	na.	0.1	0.11	0.06	0.02	0.24	25.5	20.8	0.28	0.11	na.	na.
S	0.25	0.18	0.28	0.31	0.07	0.06	0.07	0.05	5.13	5.22	0.27	0.10	na.	na.
(ppm)														
Sc	36	45	44	35	44	27	42	60	14	21	29	14	5	24
V	434	383	431	297	302	195	288	374	1391	1235	213	114	88	134
Ba	214	125	239	1475	911	408	1197	678	639	561	954	1147	14300	288
Sr	355	178	241	1015	554	281	351	223	225	70	785	1024	3717	636
Y	34.9	24.2	34.5	6	17	10	15	23	42	26	16	9	35	13
Zr	178	71	120	101	155	101	101	109	125	115	125	163	1304	217
Cr	80	130	100	530	420	360	380	580	70	130	270	50	bdl.	250
Co	38	53	48	35	36	28	31	49	18	27	30	17	4	31
Ni	39	64	54	140	180	140	160	240	130	160	120	bdl.	bdl.	50
Cu	40	33	76	70	20	20	20	20	330	330	50	30	20	bdl.
Zn	121	89	120	150	120	80	160	160	1230	860	160	100	40	210
Rb	4	7	4	65	72	45	90	79	66	56	47	35	44	10
Nb	8.7	4.5	7.9	5	6	4	5	6	4	5	5	6	12	13
Mo	bdl.	bdl.	2	bdl.	2	bdl.	bdl.	2	77	65	bdl.	2	bdl.	bdl.
La	12.3	8.94	18.4	9.6	14.5	13.4	14.9	12.5	29.4	31.7	48.7	39.5	255	30.7
Ce	29	20.3	41.3	16.9	27.2	26.1	29.6	23.8	51.3	55.8	99.8	78.2	642	67.7
Pr	3.92	2.68	5.3	1.89	3.01	2.93	3.44	2.74	7.22	7.23	11.3	8.92	81.9	8.08
Nd	18.4	12.1	23.3	7.4	11.4	11.7	14.3	10.7	28.9	27.7	44.9	35.6	324	32.4
Sm	5.38	3.18	5.58	1.3	2.6	2.3	3.3	2.8	6.4	5.3	8	6.2	44.8	5.9
Eu	1.6	1.2	1.75	1.34	1.38	0.89	1.19	0.91	1.79	1.37	1.86	2.3	11.1	1.64
Gd	6.16	3.84	5.91	1.2	3	2.2	3.2	3.9	6.4	4.6	5.4	4.3	20.5	4.2
Tb	1.1	0.71	1	0.2	0.6	0.3	0.6	0.8	1.1	0.8	0.7	0.6	1.9	0.6
Dy	6.43	4.62	6.48	1.4	3.5	2	3.4	4.9	6.7	4.7	3.5	2.7	7.9	3.1
Ho	1.34	0.91	1.23	0.3	0.7	0.4	0.6	0.9	1.4	1	0.6	0.4	1.2	0.6
Er	3.83	2.62	3.65	1	2.1	1.2	1.9	2.8	4.1	3.2	1.7	1.1	2.9	1.5
Tm	0.535	0.377	0.523	0.19	0.32	0.18	0.28	0.45	0.63	0.52	0.24	0.14	0.36	0.21
Yb	3.45	2.5	3.43	1.3	2.3	1.2	2.2	2.7	4.7	3.6	1.6	0.8	2.1	1.3
Lu	0.533	0.406	0.552	0.23	0.35	0.19	0.33	0.46	0.76	0.57	0.24	0.13	0.33	0.22
Hf	4.1	1.9	3	2.2	2.9	2.5	2.3	2.8	3	2.6	2.6	3.4	20.5	4.4
Ta	0.63	0.33	0.57	0.2	0.3	0.3	0.4	0.4	0.4	0.5	0.3	0.3	0.7	0.6
Th	0.91	0.66	1.95	0.5	0.7	0.8	2.3	2.3	5.2	5.6	6.5	1.2	11.3	0.4
U	0.69	0.3	1.27	0.5	0.5	0.4	0.9	0.6	47.1	53.6	1.4	0.6	2.9	1.4
Mg#	0.40	0.48	0.47	0.56	0.50	0.52	0.49	0.48	0.19	0.28	0.49	0.45	0.43	0.57
ASI	0.52	0.60	0.47	1.06	1.20	0.99	1.13	1.44	1.08	1.60	0.92	0.92	0.87	1.34
(La/Yb) _n	2.4	2.4	3.6	5.0	4.3	7.6	4.6	3.1	4.2	6.0	20.7	33.5	82.5	16.0
Eu/Eu*	0.84	1.05	0.92	3.21	1.50	1.19	1.10	0.84	0.84	0.83	0.81	1.29	0.97	0.96

Abbreviations: bdl., below detection limit; Chl, chloritized; Gn, gneiss; Gr, graphite; Grt, garnet; Hbl, hornblende; Hem, hematized; Met, metasomatized; na., not analyzed; Opx, orthopyroxene.

Table 2: Summary of Sm-Nd isotopic data for select rock samples from the Huzyk Creek property.

Sample number	Rock type	Sm (ppm)	Nd (ppm)	$^{147}\text{Sm}/^{144}\text{Nd}^{(1)}$	$^{143}\text{Nd}/^{144}\text{Nd}^{(2)}$	$\epsilon_{\text{Nd}}^{(3)}$ (1.90 Ga)	$T_{\text{CR}}^{(4)}$ (Ga)
108-19-HZ08	Grt wacke	2.04	6.44	0.192	0.512488 (10)	-1.7	n/a
108-19-HZ11	Opx wacke	2.60	10.56	0.149	0.512011 (10)	-0.5	n/a
108-19-HZ18	Opx wacke	2.24	11.44	0.118	0.511674 (10)	0.3	2.37
108-19-HZ20	Hbl gneiss	3.23	11.93	0.164	0.512359 (11)	2.7	n/a

Notes:

⁽¹⁾ Estimated error is better than 0.5%

⁽²⁾ Presented relative to $^{143}\text{Nd}/^{144}\text{Nd} = 0.511850$ for the La Jolla standard; numbers in parenthesis are the 2σ uncertainties $\times 10^{-6}$

⁽³⁾ ϵ_{Nd} values at 1.9 Ga calculated using present-day chondritic ratios of $^{143}\text{Nd}/^{144}\text{Nd} = 0.512638$ and $^{147}\text{Sm}/^{144}\text{Nd} = 0.1967$

⁽⁴⁾ Crustal residence Nd model ages (T_{CR}) calculated according to the linear model of Goldstein et al. (1984)

Abbreviations: Hbl, hornblende; Grt, garnet; n/a, not available; Opx, orthopyroxene.

plasma–mass spectrometry (ICP-MS) for the remainder of the trace elements and rare-earth elements (REE). Samples of the wacke-mudstone package were analyzed for carbon and sulphur, through induction-furnace combustion and measurement of the release of CO_2 and SO_2 by infrared spectrometry. Samples of hornblende gneiss and calcsilicate were analyzed by total-digestion ICP-OES for selected trace elements (Ag, Cd, Cu, Ni, Pb, Zn) and sulphur contained within sulphides.

Because of the high metamorphic grade, the wacke-mudstone package was subjected to intense partial melting. Therefore, wacke-mudstone samples were selected that appear representative of the bulk composition in terms of proportion of leucosome to melanosome or mesosome, and care was taken to avoid apparent injected leucosome in favour of material that appeared to consist of in situ or in-source leucosome. The hornblende gneiss and calcsilicate underwent minimal partial melting, so care was taken to sample material with little to no leucosome. The use of trace elements is restricted to those interpreted as less mobile in the high-grade metamorphic environment, including selected transition metals (Sc, V, Cr, Ni), high-field-strength elements (HFSE; Ti, Zr, Nb), REE and Th. However, it should be noted that Th may partition into silicate melt, the removal of which could result in the depletion of Th.

Samples of wacke from immediately above and below the graphite-rich horizons, as well as one sample of hornblende gneiss, were submitted for Sm-Nd isotope geochemical analysis to the University of Alberta Radiogenic Isotope Facility (Edmonton, Alberta). The rock-sampling and initial-processing procedures followed were the same as those for litho-geochemistry samples. The samples were processed and analyzed for Sm-Nd isotopes following the chromatographic and mass-spectrometry methods outlined by Unterschutz et al. (2002) and Schmidberger et al. (2007). Samarium and neodymium isotopic compositions were determined by multicollector (MC)-ICP-MS, for which an in-house Nd isotope standard was used (Schmidberger et al., 2007). Chemical processing blanks were <200 pg for Nd and Sm. The Nd data are presented relative to a $^{143}\text{Nd}/^{144}\text{Nd}$ value of 0.511850 for the La Jolla standard, and crustal resi-

dence model ages (T_{CR}) were calculated based on the model of Goldstein et al. (1984), which assumes a linear evolution of isotopic ratios in the depleted mantle, using present-day depleted-mantle values of $^{143}\text{Nd}/^{144}\text{Nd} = 0.513160$ and $^{147}\text{Sm}/^{144}\text{Nd} = 0.2141$. Initial ϵ_{Nd} values cited in the text were calculated at 1.90 Ga.

Hornblende gneiss and calcsilicate

The hornblende gneiss is mafic ($\text{SiO}_2 = 48\text{--}51\%$) with Mg# values of 0.40–0.49 (molar $\text{Mg}/[\text{Mg}+\text{Fe}]$). The samples also plot within the basalt field of the Zr/Ti-Nb/Y diagram of Pearce (1996), suggesting that these rocks represent metamorphosed basalt flows and/or mafic intrusions (Figure 8a). Chondrite-normalized REE-profiles have gentle negative slopes (Figure 8b), although one sample is relatively steeper than the other two ($[\text{La}/\text{Yb}]_{\text{N}} = 7.7$ vs. 2.4). Primitive mantle-normalized multi-element profiles have negative slopes with two of the samples displaying slight depletions at Th, Nb, and Ti (Figure 8c). The sample with the higher $(\text{La}/\text{Yb})_{\text{N}}$ ratio is characterized by a much steeper sloping LREE profile, and more pronounced negative anomalies at Nb, Zr, and Ti. Discrimination diagrams suggest the hornblende gneiss is transitional between tholeiitic continental-arc basalt and calcalkaline basalt (Figure 9a–d). One sample of hornblende gneiss yielded an initial ϵ_{Nd} value of +2.7.

The silica and Mg# values for the calcsilicate are similar to the hornblende gneiss ($\text{SiO}_2 = 48\text{--}50\%$, $\text{Mg\#} = 0.37\text{--}0.47$). Normalized REE-profiles of the calcsilicate have a negative slope similar to the hornblende gneiss ($[\text{La}/\text{Yb}]_{\text{N}} = 2.2\text{--}3.6$; Figure 8d), as do the normalized multi-element profiles (Figure 8e). One sample of the calcsilicate is characterized by a slightly steeper sloping LREE-profile, and more pronounced negative anomalies at Nb, Zr, and Ti, when compared to the other two calcsilicate samples. The similarity in geochemistry, combined with the closely interbanded relationship between the calcsilicate and the hornblende gneiss suggest a common protolith. The Zr/TiO₂-Ni discrimination diagram can be used with certain caveats to distinguish metamorphic rocks derived from an igneous protolith, from rocks derived from a sedimentary protolith (Couëslan, 2018a). The hornblende gneiss and calcsilicate

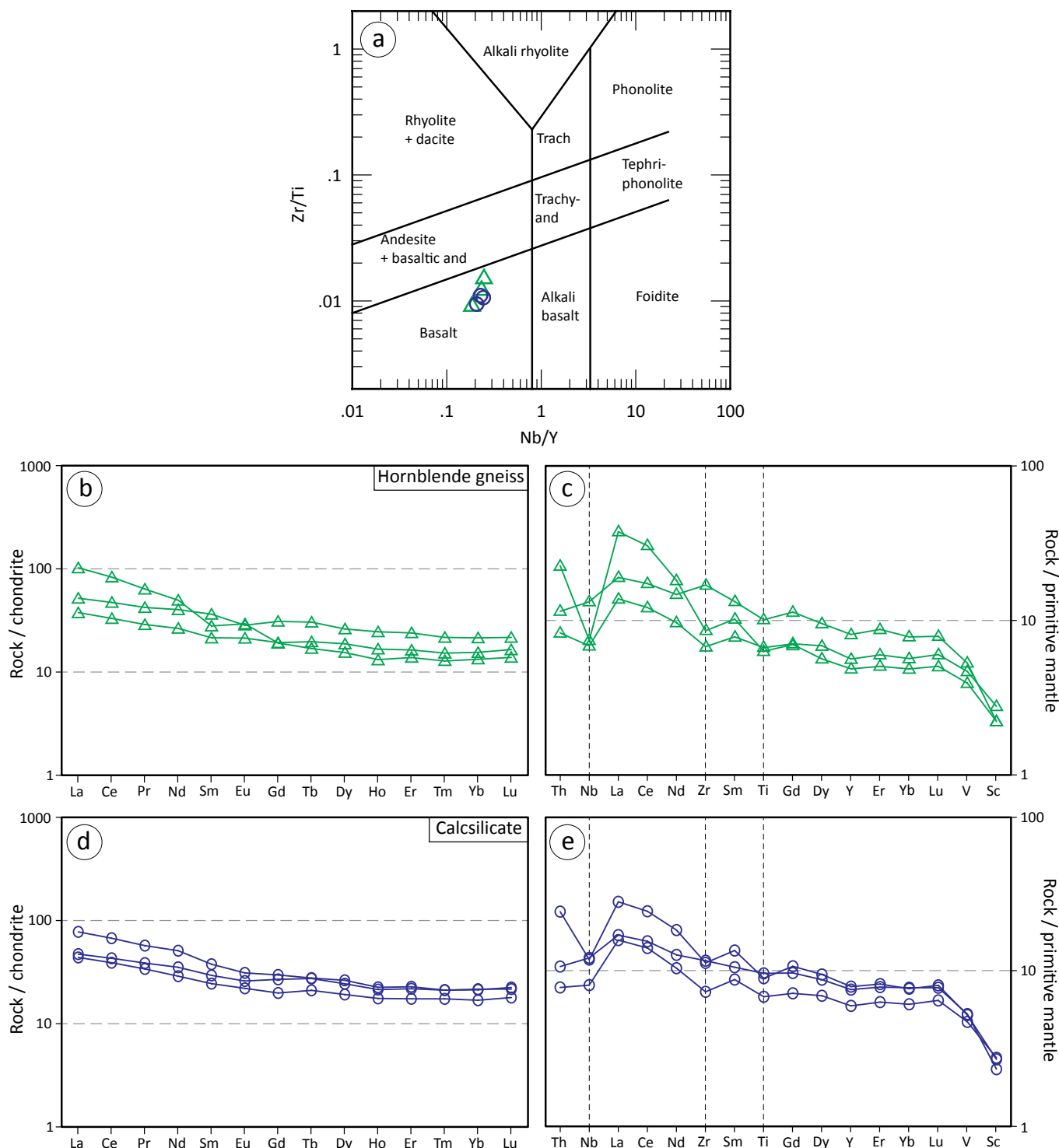


Figure 8: Geochemical diagrams for the hornblende gneiss and calcsilicate: **a)** composition of the hornblende gneiss and calcsilicate plotted on the Zr/Ti-Nb/Y diagram of Pearce (1996); **b)** chondrite-normalized REE profiles and **c)** primitive mantle-normalized multi-element profiles of the hornblende gneiss; **d)** chondrite-normalized REE profiles and **e)** primitive mantle-normalized multi-element profiles of the calcsilicate. Normalizing values for chondrite and primitive mantle are from McDonough and Sun (1995). Abbreviation: and, andesite; Trach, trachyte.

plot as a cluster within the igneous protolith field (Figure 9e). This further supports the idea that these two units are likely derived from a common protolith. The calcsilicate also plots in close association with the hornblende gneiss on the Zr/Ti-Nb/Y discrimination diagram of Pearce (1996; Figure 8a), as well as other discrimination diagrams (Figure 9a-d), suggesting

a tholeiitic-continental arc basalt- to calcalkaline basalt-affinity for the calcsilicate.

Wacke-mudstone

All samples of the wacke-mudstone package plot within the sedimentary protolith field of the Zr/TiO₂-Ni discrimina-

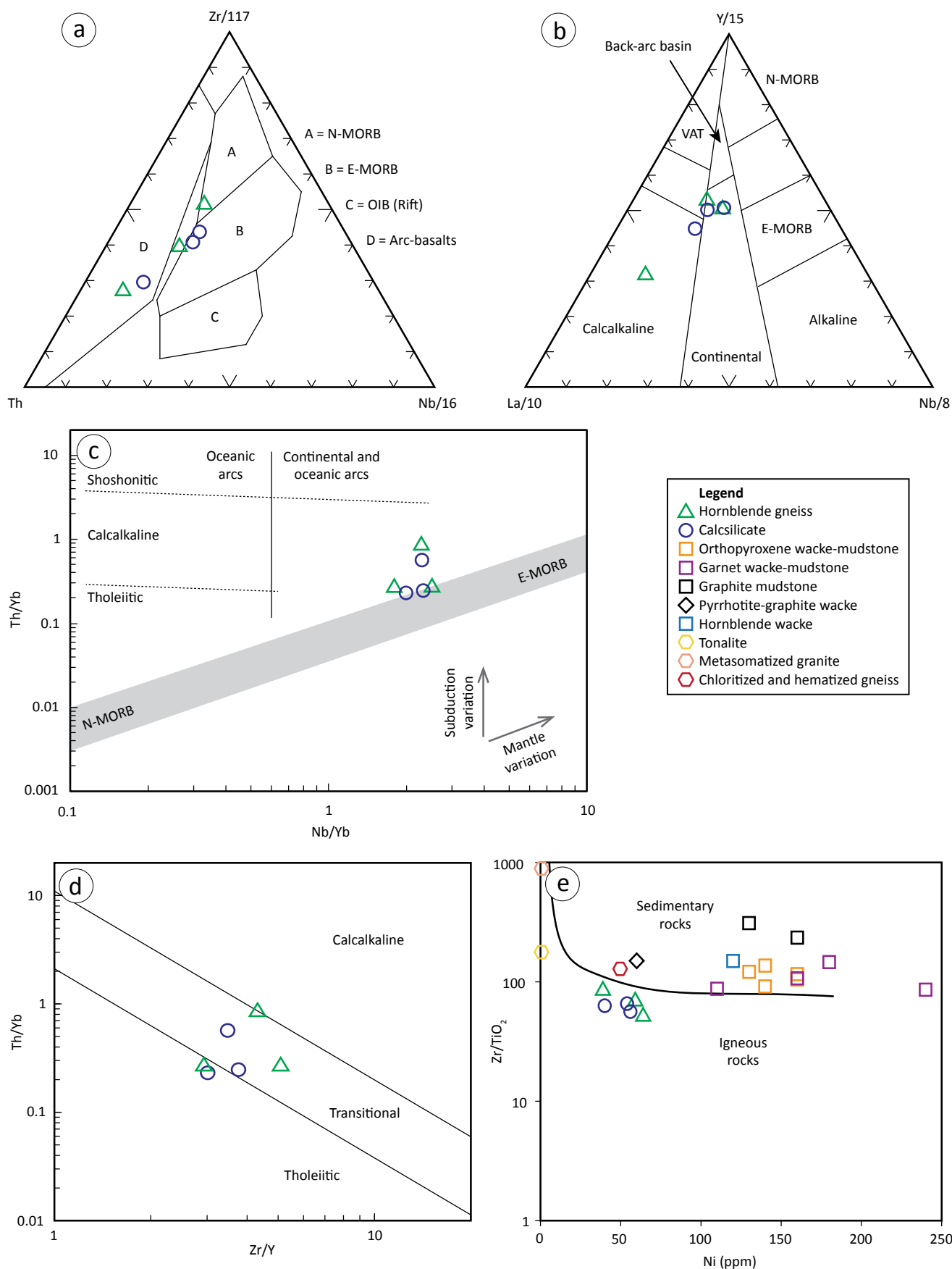


Figure 9: Discrimination diagrams for rocks of the Huzyk Creek property: **a)** Th-Zr-Nb diagram of Wood (1980); **b)** La-Y-Nb diagram of Cabanis and Lecolle (1989); **c)** Th/Yb-Nb/Yb diagram of Anderson (2008; modified after Pearce and Peate, 1995); **d)** Th/Yb-Zr/Y diagram of Ross and Bédard (2009); **e)** Zr/TiO₂-Ni diagram of Couëslan (2018, modified from Winchester et al., 1980). Abbreviations: E-MORB, enriched mid-ocean-ridge basalt; N-MORB, normal mid-ocean-ridge basalt; OIB, oceanic-island basalt; VAT, volcanic-arc tholeiite.

tion diagram (Figure 9e). The orthopyroxene wacke-mudstone is weakly metaluminous to peraluminous ($ASI = 0.99\text{--}1.27$; molar $Al_2O_3/[CaO+Na_2O+K_2O]$) with $Mg\#$ values of $0.50\text{--}0.61$. The garnet wacke-mudstone is typically more aluminous ($ASI = 1.13\text{--}1.44$) and less magnesian ($Mg\# = 0.43\text{--}0.49$), while the one sample of hornblende wacke is metaluminous ($ASI = 0.92$) with and $Mg\#$ of 0.49 . The graphite mudstone-wacke samples are peraluminous ($ASI = 1.08\text{--}1.60$). The graphitic mudstones are enriched in iron compared to the other rocks of the wacke-mudstone package ($Mg\# = 0.19\text{--}0.28$), which is a function of their elevated sulphide content.

Whole-rock geochemical data for the wacke were normalized to the average P2 member pelite of the Pipe formation and plotted on multi-element diagrams, as outlined in Zwanzig et al. (2007). The normalized multi-element profiles of the orthopyroxene wacke-mudstone and garnet wacke-mudstone are broadly similar with positive slopes, enrichments at Nb, Ti, V, Sc, and Cr, and minor depletion at Y (Figure 10a, b). Profiles for the orthopyroxene wacke-mudstone display greater variability in REE content than the garnet wacke-mudstone and can have positive anomalies at Zr. The profile of the pyrrhotite-graphite wacke is similar to that of the orthopyroxene and garnet wacke-mudstones, except for relatively greater Th content, and no positive anomaly at Nb. The graphite mudstone profile is similar to the other wacke-mudstones but with overall

higher Th and REE content, a strong positive anomaly at V, and negative anomalies at Zr, Ti, and Al. Uranium is not included in the element suite because of potential element mobility; however, it should be noted that U in the graphite mudstone is enriched by three orders of magnitude relative to the other wacke-mudstones (Table 1). The hornblende wacke profile has a gentle negative slope because of slight enrichment of the LREE. It is depleted at Th, Nb, Zr, and Ti, and enriched in V, Sc, and Cr.

One sample of orthopyroxene wacke yielded a crustal-residence Nd-model age of 2.37 Ga, while the two remaining wacke-mudstone samples did not yield results suitable for calculating model ages ($^{147}Sm/^{144}Nd > 0.14$). The two samples of orthopyroxene wacke yielded initial ϵ_{Nd} values of $+0.3$ and -0.5 . The garnet wacke sample yielded a slightly more evolved ϵ_{Nd} value of -1.7 .

Intrusions

The tonalite is metaluminous ($ASI = 0.92$) with an $Mg\#$ of 0.45 . It is relatively enriched in Ba (1147 ppm) and Sr (1024 ppm). The chondrite-normalized REE profile has a moderate negative slope ($[La/Yb]_N = 34$) with a weak positive Eu anomaly ($Eu^*/Eu = 1.3$; Figure 11a). The primitive mantle-normalized multi-element profile is characterized by negative anomalies

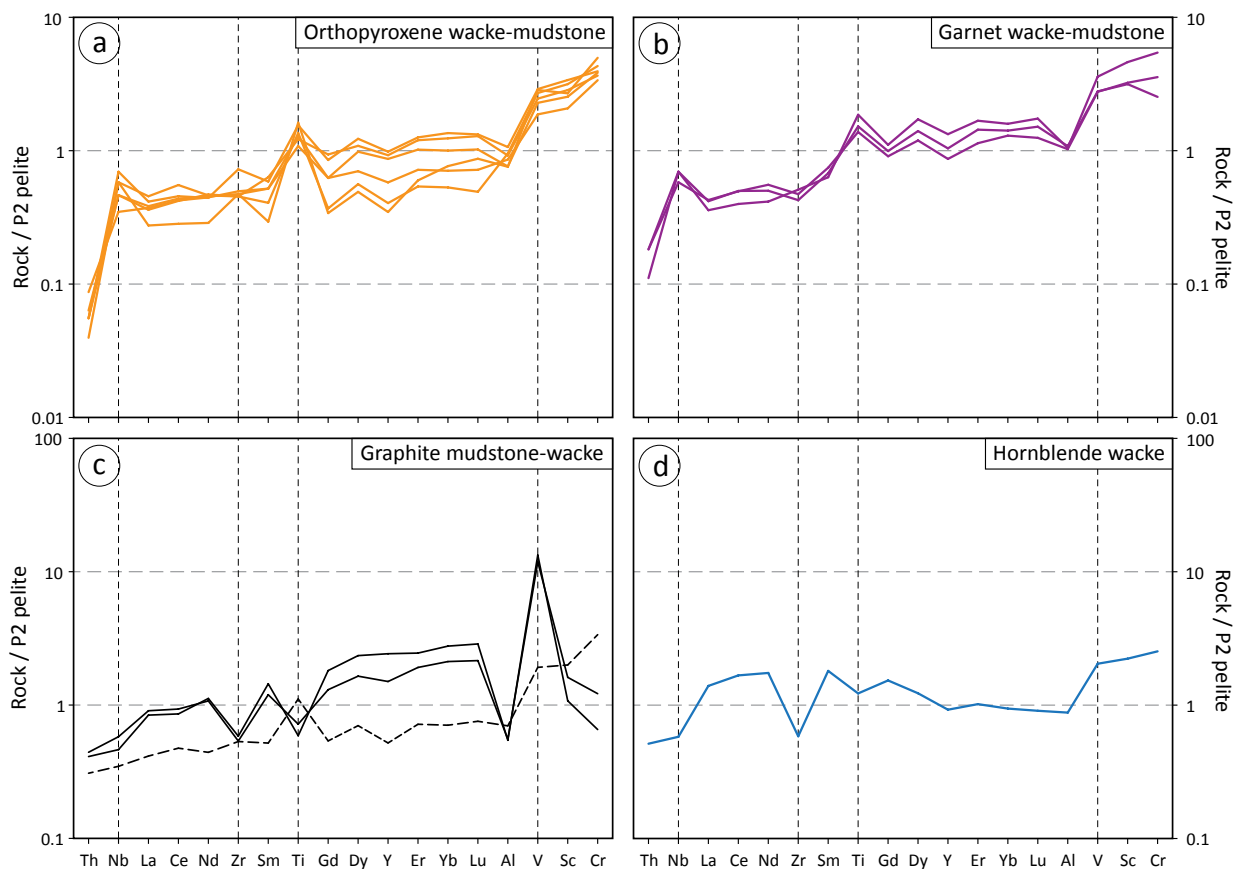


Figure 10: Multi-element profiles of wacke-mudstones normalized to average P2 pelite of Zwanzig et al. (2007): **a)** orthopyroxene wacke-mudstone; **b)** garnet wacke-mudstone; **c)** graphite mudstone-wacke, solid lines indicate graphite mudstone, dashed line indicates pyrrhotite-graphite wacke; **d)** hornblende wacke-mudstone. Note difference in y-axes scales between figures a) and b), and figures c) and d).

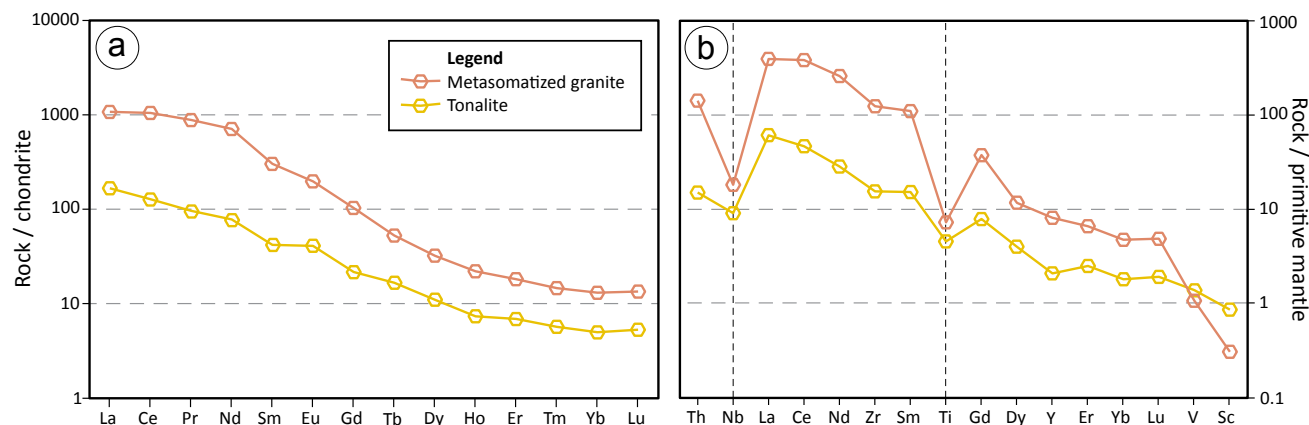


Figure 11: Chondrite-normalized rare-earth element profiles **(a)** and primitive mantle-normalized multi-element profiles **(b)** for tonalite and metasomatized granite from Huzyk Creek. Normalizing values are from McDonough and Sun (1995).

at Nb and Ti suggesting an arc- or crustal melt-derived affinity (Figure 11b).

The metasomatized granite is metaluminous ($ASI = 0.87$) with an $Mg\#$ of 0.43. It is strongly enriched in Ba (14 300 ppm), Sr (3717 ppm), Zr (1304 ppm), and LREE ($\Sigma LREE = 1303$ ppm; Table 1). The chondrite-normalized REE profile has a steep negative slope ($[La/Yb]_N = 82$) that is shallower at either terminus (Figure 11a). The primitive mantle-normalized profile has strong negative anomalies at Nb and Ti suggesting an arc- or crustal-melt-derived affinity (Figure 11b).

Chloritized and hematized gneiss

The chloritized and hematized gneiss is relatively mafic ($SiO_2 = 47.47\%$) and peraluminous ($ASI = 1.34$) with an $Mg\#$ value of 0.57. The gneiss plots within the sedimentary protolith field on the Zr/TiO_2 -Ni diagram close to the pyrrhotite-graphite wacke, but is also in proximity to the cluster of points defined by the hornblende gneiss and calcsilicate (Figure 9e). A primitive mantle-normalized profile of the gneiss has a moderate negative slope with relative depletions at Th and Nb (Figure 12a). Normalizing to P2 yielded a profile that is relatively flat, with a strong negative anomaly at Th, and enrichments at Nb, Ti, V, Sc, and Cr (Figure 12b).

Metamorphism

Phase equilibrium modelling was conducted on the least retrogressed hornblende gneiss sample, and all wacke-mudstone samples, excluding the graphitic mudstone-wackes. Discussion will be limited to the hornblende gneiss (108-19-HZ20), and two samples of orthopyroxene wacke-mudstone (108-19-HZ14 and 108-19-HZ15), which provided the best constraints for peak metamorphic temperature and pressure.

Methods

Petrographic thin sections of the samples were examined and modal abundances were calculated based on >650 point counts for each thin section (point count results available in

Appendix 3). Observed modal abundances were later compared to the predicted modal abundances to ensure a close fit between observed and modelled mineral assemblages. Phase equilibrium diagrams were calculated using the Theriak-Domino software package (de Capitani and Brown, 1987; de Capitani and Petrakakis, 2010), and using the updated ds5.5 thermodynamic dataset of Holland and Powell (1998). The activity models used are those outlined in Tinkham and Ghent (2005) and Pattison and Tinkham (2009), with the following exceptions: (i) the monoclinic amphibole model is that of Diener et al. (2007), (ii) the biotite model is that of White et al. (2007), (iii) the garnet model is that of White et al. (2007) with the Margules parameters of almandine-grossular and pyrope-grossular following THERMOCALC v.3.31 data files, (iv) the spinel model is that of White et al. (2002), and (v) the liquid model is that of White et al. (2007) with the enthalpy of forsterite and fayalite liquid adjusted by -10 kJ/mol and -9 kJ/mol, respectively, following THERMOCALC v.3.31 data files. Samples were modelled in the chemical system NCKFMASHT (Na_2O - CaO - K_2O - FeO - MgO - Al_2O_3 - SiO_2 - H_2O - TiO_2) and projected from pyrrhotite and apatite. The chemical system was oversaturated with a pure H_2O fluid phase below the solidus. Above the solidus the H_2O content of each model is restricted to the maximum amount of H_2O contained in the solid phases <0.5°C below the solidus within the modelled pressure range of the diagram. The H_2O content in the system at the temperature of melting is therefore at the approximate point of saturation (White et al., 2001).

Mineral assemblages

Hornblende gneiss sample 108-19-HZ20 is medium to coarse grained and granoblastic with an assemblage of hornblende-plagioclase-clinopyroxene-orthopyroxene-ilmenite-biotite. Apatite and pyrrhotite occur as accessory phases. Orthopyroxene occurs as part of the groundmass and as local, coarse porphyroblasts (Figure 13a). Exsolution lamellae of orthopyroxene and/or pigeonite are common within clinopy-

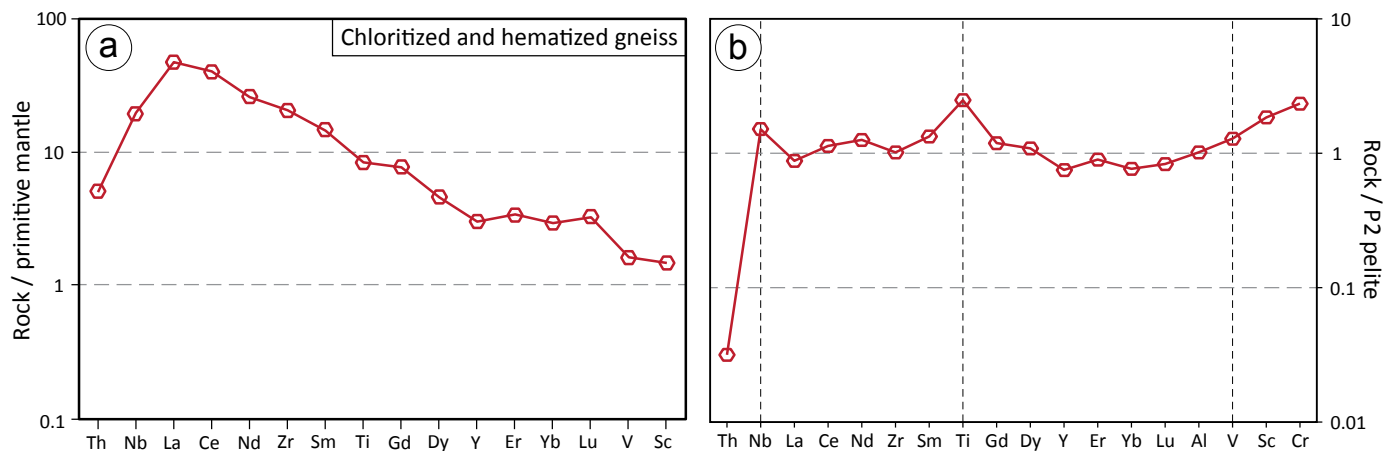


Figure 12: Multi-element diagrams of the chloritized and hematized gneiss normalized to primitive mantle (a) and average P2 pelite (b). The normalizing values for primitive mantle are from McDonough and Sun (1995), and for average P2 pelite from Zwanig et al. (2007).

roxene (Figure 13b). Contacts between ilmenite and pyroxene are commonly lined by thin envelopes of hornblende. Fine-grained biotite is typically associated with, and often partially envelopes, ilmenite. Local, discontinuous coarse-grained domains are dominated by plagioclase and pyroxene and lined by hornblende-rich selvages. These domains could represent zones of recrystallized leucosome. This may be supported by the rare occurrence of very fine biotite-quartz symplectite, a subsolidus texture that is common in migmatitic rocks (Waters, 2001; Sawyer, 2008). The mineral assemblage hornblende-plagioclase-clinopyroxene-orthopyroxene-ilmenite is typical for a mafic rock of the lower granulite-facies (Pattison et al., 2003).

Rocks of the wacke-mudstone suite are metatexites with well-developed leucosome and preserved sedimentary layering. Orthopyroxene wacke sample 108-19-HZ14 is medium grained and foliated with an assemblage of plagioclase-quartz-biotite-cummingtonite-ilmenite. Apatite, K-feldspar, graphite, pyrrhotite, and zircon occur as accessory phases. Cummingtonite occurs as fine- to medium-grained intergrowths that pseudomorphously replaced poikiloblastic orthopyroxene (Figure 13c). Fine-grained biotite-quartz symplectite is locally intergrown with the cummingtonite and is also likely a replacement of orthopyroxene.

Orthopyroxene mudstone sample 108-19-HZ15 is medium grained and foliated with an assemblage of plagioclase-biotite-orthopyroxene-quartz-garnet-K-feldspar-ilmenite. Apatite, pyrrhotite, and graphite occur as accessory phases. Sparse grains of antiperthite are present (Figure 13d). Although garnet and orthopyroxene occur together, they generally occur in alternating garnet-rich and orthopyroxene-rich layers. Orthopyroxene is locally oriented with the rock fabric suggesting peak metamorphism was attained during, or prior to, the generation of the penetrative foliation. Fine- to medium-grained K-feldspar forms interstitial networks in plagioclase-rich domains, which may in part be pseudomorphous after melt films (Figure 13e; Holness and Sawyer, 2008; Holness et

al., 2011). Potassium feldspar can be partially or completely replaced by very fine-grained myrmekite and biotite-quartz symplectite. Biotite-quartz symplectite also occurs as a replacement of orthopyroxene (Figure 13f). The mineral assemblage orthopyroxene-plagioclase-melt-garnet-K-feldspar is characteristic of granulite-facies psammitic to semipelitic rocks (Pattison et al., 2003).

Phase equilibrium modelling

The phase diagram section for hornblende gneiss sample 108-19-HZ20 provides fairly well constrained temperature and pressure conditions for the observed mineral assemblage hornblende-plagioclase-clinopyroxene-orthopyroxene-ilmenite-biotite. The equilibrium assemblage containing hornblende-clinopyroxene-orthopyroxene-ilmenite-melt defines a field in pressure-temperature space of 5.6–7.3 kbar and 750–810°C (Figure 14a).

Orthopyroxene wacke sample 108-19-HZ14 contains the mineral assemblage plagioclase-quartz-biotite-cummingtonite-ilmenite. The cummingtonite is interpreted to be pseudomorphous after orthopyroxene. The equilibrium assemblage containing orthopyroxene-biotite-ilmenite-quartz-melt defines a relatively broad field in pressure-temperature space from <2.0 to 9.0 kbar and 750 to 880°C (Figure 14b). Orthopyroxene mudstone sample 108-19-HZ15 contains the mineral assemblage plagioclase-biotite-orthopyroxene-quartz-garnet-K-feldspar-ilmenite. The equilibrium assemblage containing orthopyroxene-garnet-ilmenite-quartz-melt also defines a relatively broad field in pressure-temperature space from 5.3 to >10 kb and 730 to >860°C (Figure 14c).

Individually, the equilibrium assemblage diagrams for the orthopyroxene wacke and mudstone provide rather poor pressure-temperature constraints; however, overlaying the two observed equilibrium-assemblage fields defines a better constrained pressure-temperature range of about 5.3–8.3 kbar and 760–840°C (Figure 14d). This pressure-temperature range is consistent with results from the hornblende gneiss sample; however,

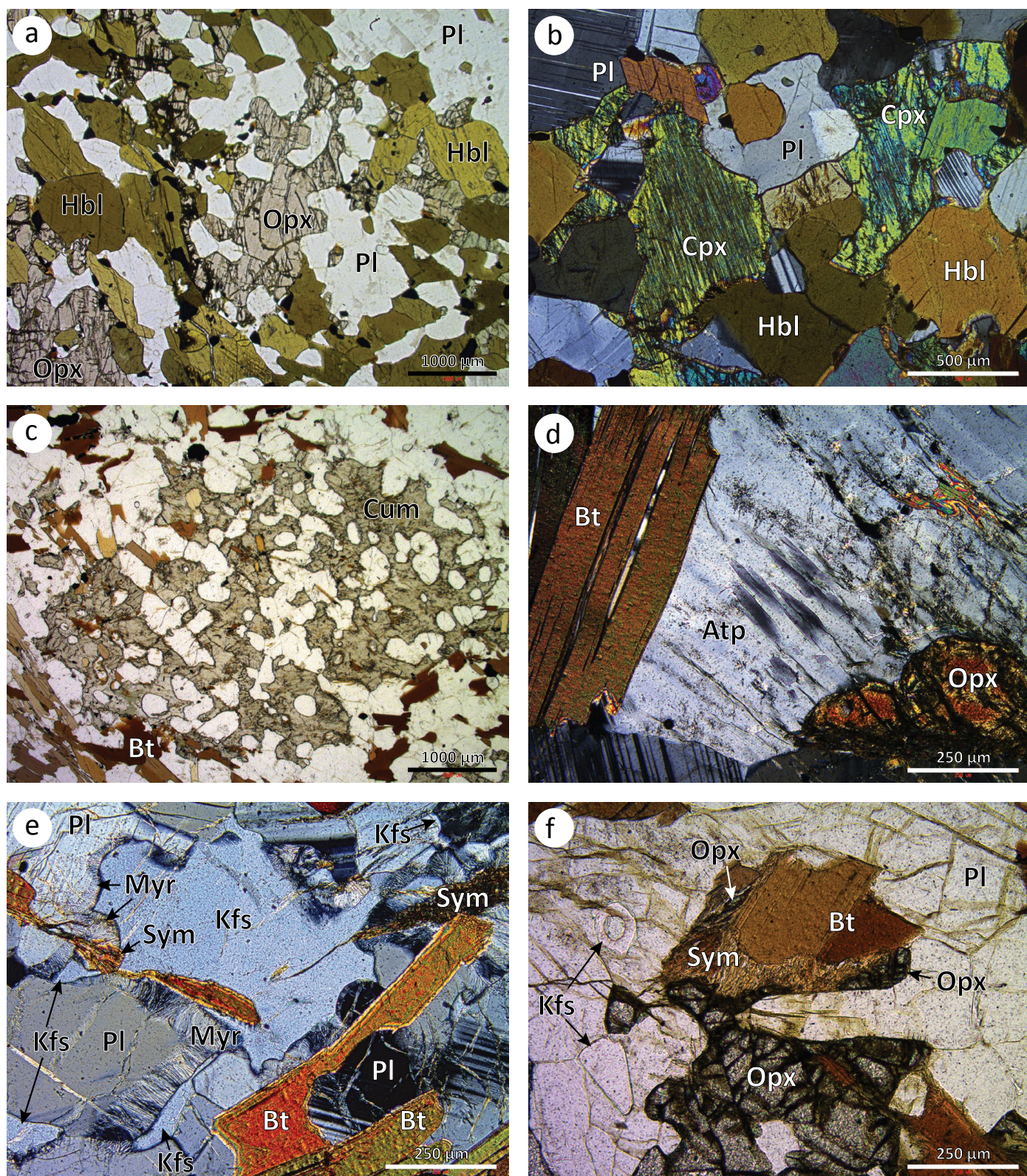


Figure 13: Photomicrographs of hornblende gneiss and wacke-mudstone samples: **a)** orthopyroxene porphyroblasts in hornblende gneiss (plane-polarized light; sample 108-19-HZ20); **b)** clinopyroxene with exsolution lamellae of orthopyroxene and/or pigeonite in hornblende gneiss (cross-polarized light; sample 108-19-HZ20); **c)** orthopyroxene pseudomorph consisting of polycrystalline cummingtonite, in orthopyroxene wacke (plane-polarized light; sample 108-19-HZ14); **d)** antiperthitic plagioclase in orthopyroxene mudstone (cross-polarized light; sample 108-19-HZ15); **e)** K-feldspar interstitial to plagioclase in orthopyroxene mudstone, myrmekite and local biotite-quartz symplectite are present along the periphery of the K-feldspar (cross-polarized light; sample 108-19-HZ15); **f)** orthopyroxene overprinted by biotite-quartz symplectite in orthopyroxene mudstone (plane-polarized light; sample 108-19-HZ15). Abbreviations: Atp, antiperthite; Bt, biotite; Cpx, clinopyroxene; Cum, cummingtonite; Hbl, hornblende; Kfs, K-feldspar; Myr, myrmekite; Opx, orthopyroxene; Pl, plagioclase; Sym, biotite-quartz symplectite.

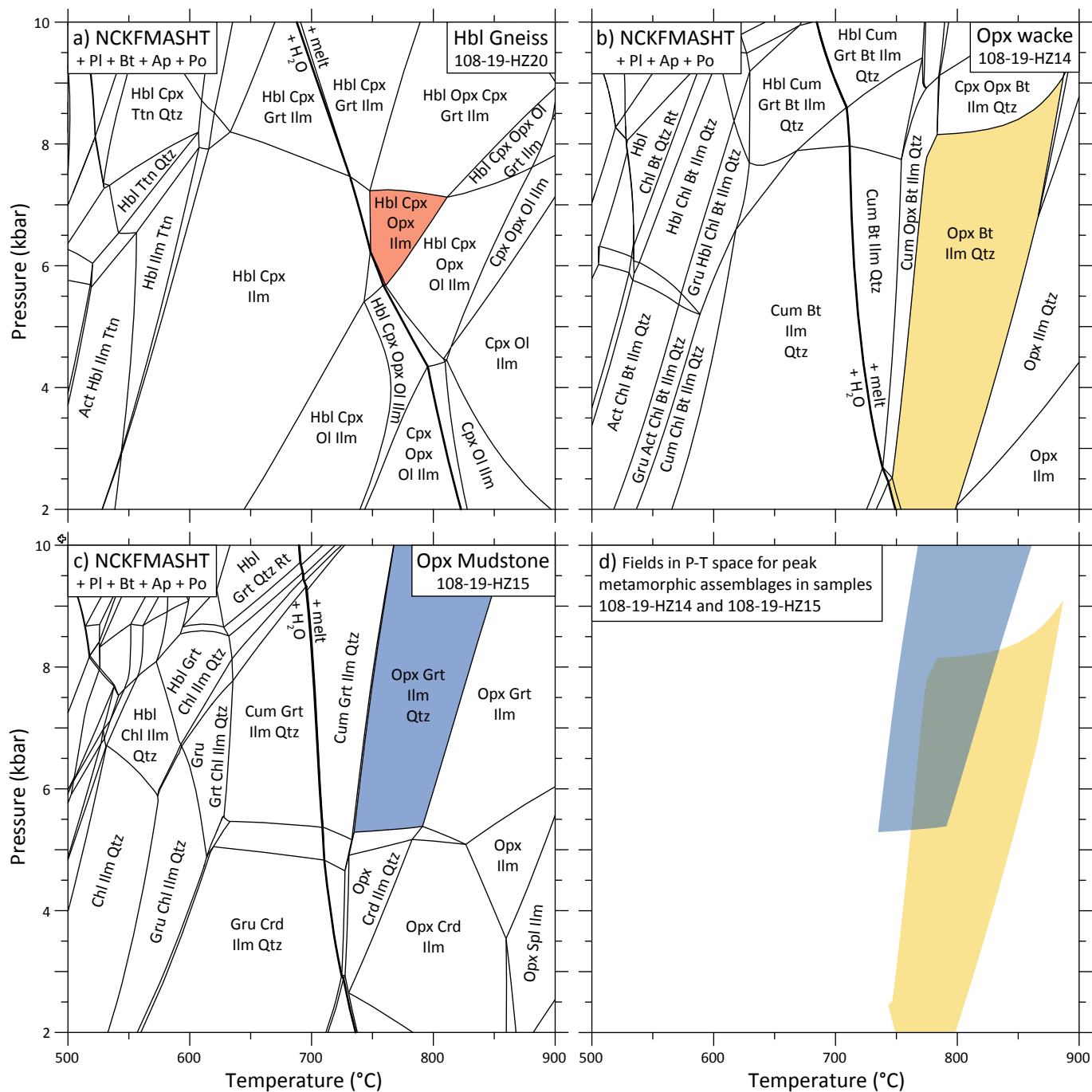


Figure 14: Phase diagram sections in NCKFMASHT for: **a)** hornblende gneiss sample 108-19-HZ20; **b)** orthopyroxene wacke sample 108-19-HZ14; **c)** orthopyroxene mudstone sample 108-19-HZ15; **d)** overlay of observed assemblage fields from samples 108-19-HZ14 and 108-19-HZ15. Coloured fields indicate the observed mineral assemblages in each sample. Abbreviations: Act, actinolite; Ap, apatite; Bt, biotite; Chl, chlorite; Cpx, clinopyroxene; Crd, cordierite; Cum, cummingtonite; Grt, garnet; Gru, grunerite; Hbl, hornblende; Ilm, ilmenite; Ol, olivine; Opx, orthopyroxene; Pl, plagioclase; Po, pyrrhotite; Qtz, quartz; Rt, rutile; Spl, spinel; Ttn, titanite.

the hornblende gneiss provides better pressure-temperature constraint and is considered the best estimate of peak metamorphic conditions at about 5.6–7.3 kbar and 750–810°C (Figure 14a).

Discussion

This section focuses on the affinity of the Huzyk Creek stratigraphy; however, a brief discussion of the intrusions and chloritized and hematized gneiss are presented first.

Intrusions and chloritized and hematized gneiss

The metasomatized granite is strongly enriched in incompatible elements (Table 1). Incompatible elements are typically concentrated in accessory phases such as titanite and allanite, which in the case of the metasomatized granite, appear to be associated with the carbonate-biotite veinlets. This suggests that the enrichment is likely related to the metasomatizing fluid, as opposed to being an original magmatic feature

of the granite. Several syenitic complexes are present in the Reindeer zone of Manitoba and are characterized by abundant metasomatic phases and enrichment of incompatible elements (Couëslan, 2005; Chakhmouradian et al., 2008; Martins, 2016a–c). Primitive mantle-normalized multi-element diagrams for metasomatized rocks from these complexes yield profiles with similar slopes, enrichments, and depletions, with the lone exception of Zr, which is less depleted in the Huzyk Creek rock (Figure 15). The multi-element profiles suggest that the metasomatized rock at Huzyk Creek and rocks associated with the various syenitic complexes in the Reindeer zone were metasomatized by fluids of similar geochemical affinity. This implies that a similar magmatic system (igneous complex) could be present in relatively close proximity to the drillholes at Huzyk Creek. Further studies are planned to investigate the prevalence of metasomatism, the possible source(s) for metasomatizing fluids, and the potential for rare-element mineralization in the Huzyk Creek drillcore.

The P2 pelite-normalized profile of the chloritized and hematized gneiss sample is distinctly different from the wacke-mudstone sequence and suggests that they are likely unrelated (Figure 16a). The primitive mantle-normalized profile of the gneiss is also distinct from the mafic rocks at Huzyk; however, it is similar to the profile of the tonalite sample (Figure 16b). The chloritized gneiss is slightly less depleted in Nb and Ti, and

more depleted in Th, suggesting a more primitive composition. Therefore, the chloritized and hematized gneiss sample could represent a more primitive magma (diorite/melatonalite?) related to the tonalite. It should be noted that the metasomatism responsible for the chloritized and hematized gneiss overprinted more than one rock type, and that additional sampling and analyses could yield a variety of multi-element profiles and rocks of varying affinities. The primitive mantle-normalized profile of the chloritized and hematized gneiss from drillhole HZ-19-2 is considerably less enriched than the metasomatized granite from drillhole HZ-19-1. In addition, the prevalence of chlorite and hematite and the presence of piemontite suggests the fluid that altered the gneiss was lower temperature and strongly oxidizing compared to the fluid that altered the granite. Therefore, the metasomatizing fluid that generated the chloritized and hematized gneiss was likely unrelated to the fluid responsible for the metasomatized granite.

Stratigraphic affinity of the wacke-mudstone sequence

The Huzyk Creek area was previously reported as being underlain by upper amphibolite-facies rocks (Beaumont-Smith, 2018); however, the orthopyroxene-bearing mineral assemblages of the hornblende gneiss and wacke-mudstone suite suggest granulite-facies metamorphism. The identification and correlation of sedimentary rocks in high-grade metamorphic

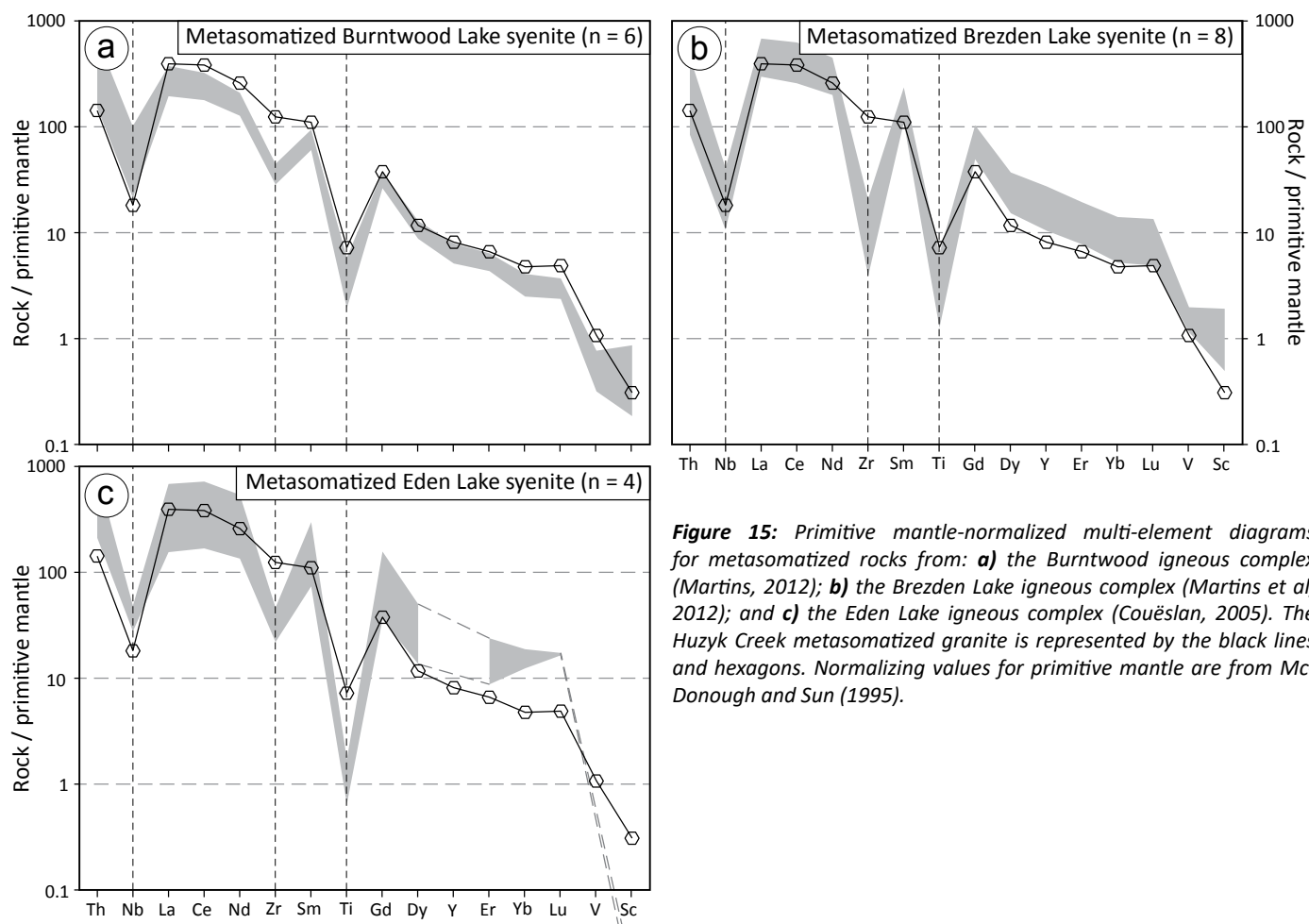


Figure 15: Primitive mantle-normalized multi-element diagrams for metasomatized rocks from: **a)** the Burntwood igneous complex (Martins, 2012); **b)** the Brezden Lake igneous complex (Martins et al, 2012); and **c)** the Eden Lake igneous complex (Couëslan, 2005). The Huzyk Creek metasomatized granite is represented by the black lines and hexagons. Normalizing values for primitive mantle are from McDonough and Sun (1995).

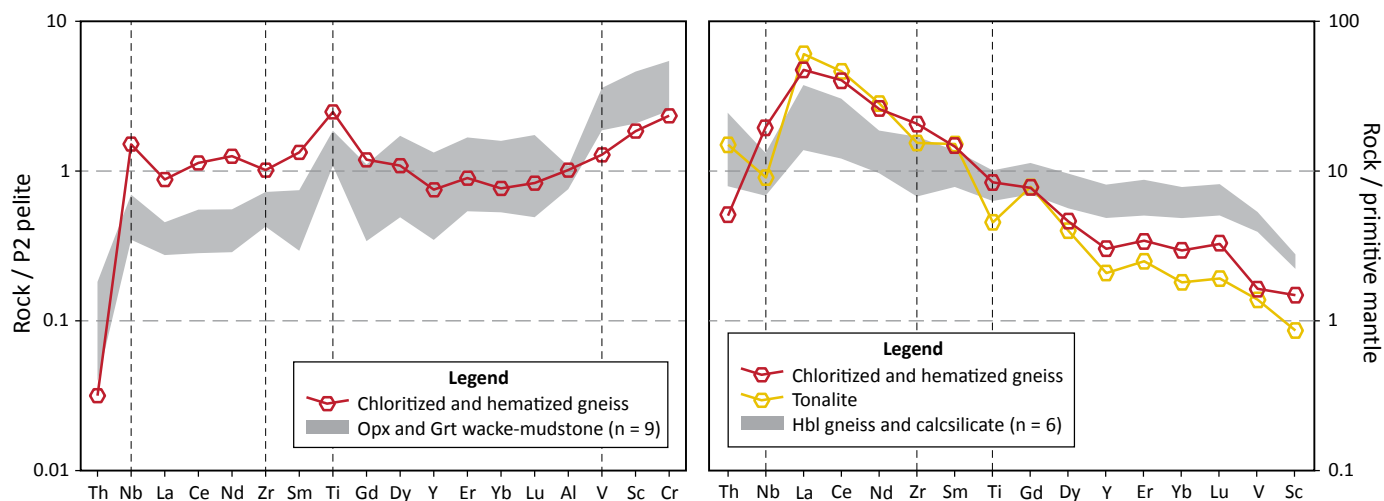


Figure 16: Multi-element diagrams of the chloritized and hematized gneiss: **a)** normalized to average P2 pelite with comparison to the wacke-mudstone sequence; **b)** normalized to primitive mantle with comparison to the hornblende gneiss and calcsilicate, and tonalite. Normalizing values for average P2 pelite are from Zwanzig et al. (2007), and for primitive mantle are from McDonough and Sun (1995). Abbreviations: Grt, garnet; Hbl, hornblende; Opx, orthopyroxene.

terranes is challenging. The identification of Oswagan group rocks in the TNB is typically made by recognizing key stratigraphic markers: arenaceous sandstones of the Manasan and Setting formations, calcsilicates and marbles of the Thompson and Pipe formations, and iron formations of the Pipe formation (Bleeker, 1990; Zwanzig et al., 2007). These rock types generally remain recognizable into granulite-facies (Zwanzig et al., 2007; Couëslan and Pattison, 2012). Although some calcsilicate is associated with the hornblende gneiss, the Huzyk Creek sequence does not correlate well with any portion of the Oswagan group stratigraphy. Average P2 pelite-normalized multi-element profiles of Oswagan group wackes and mudstones are relatively flat to weakly negative sloping, and contrast with the positive slopes of the Huzyk Creek orthopyroxene and garnet wacke-mudstones (Figure 17a–c). Oswagan group rocks are characterized by crustal-residence Nd-model ages of ca. 2.82–3.22 Ga, which implies an Archean detrital component, likely sourced from the Superior craton (Böhm et al., 2007). Although only one sample of wacke-mudstone yielded a Nd-model age, it was considerably younger at ca. 2.37 Ga. Initial ϵ_{Nd} values for the Huzyk Creek wacke-mudstone suite range from –1.7 to +0.3, which is in contrast to the range of ϵ_{Nd} values for Oswagan group rocks (–13.6 to –6.2; Figure 18; Böhm et al., 2007).

A sequence of orthopyroxene- and garnet-bearing wackes has recently been documented in the Paint and Phillips lakes area of the TNB (Paint sequence; Couëslan, 2016, 2018b). These rocks are petrographically similar to the Huzyk Creek sequence; however, they typically contain sparse interbeds of silicate-facies iron formation, a feature not observed at Huzyk Creek. Normalized multi-element profiles of the Paint sequence rocks are typically relatively flat to weakly negative sloping with pronounced enrichment of Cr (Figure 17d). Although the Huzyk Creek wacke-mudstones are enriched in Cr, the profiles are also enriched in V and Sc, and characterized

by positive slopes. Similar to the Oswagan group, the Paint sequence is characterized by Archean Nd-model ages ($T_{\text{CR}} = 2.95\text{--}3.57$ Ga) and evolved ϵ_{Nd} values (–17.8 to –9.5; Figure 18; Couëslan, 2016, unpublished data, 2018). Therefore, the Huzyk Creek sequence does not appear to correlate with the Oswagan group or Paint sequence of the TNB.

The Sm–Nd isotope geochemistry of the Huzyk Creek wacke-mudstone is more comparable with sedimentary rocks of the Trans-Hudson orogen (Burntwood group, $T_{\text{CR}} = 2.2\text{--}2.6$ Ga, $\epsilon_{\text{Nd}} = -1.7$ to +3.9; Sickle and Grass River groups, $T_{\text{CR}} = 2.0\text{--}2.4$ Ga, $\epsilon_{\text{Nd}} = -0.7$ to +4.3; Figure 18; Böhm et al., 2007). The Burntwood group consists of a thick sequence of interbedded wacke and mudstone. Upper amphibolite- to granulite-facies Burntwood group wacke typically consists of garnet-biotite gneiss, with more aluminous mudstone layers containing additional biotite±sillimanite and cordierite (e.g., Martins and Couëslan, 2019). Graphite is typically present in trace to minor amounts, although significant intersections of graphite have been reported from drillcore in the Kisseynew basin (e.g., Callinix Mines Inc., 2014; Assessment File 93001). Significant portions of the Huzyk Creek wacke-mudstone package are devoid of garnet, which could be considered atypical for Burntwood group rocks. The absence of sillimanite and cordierite from mud-rich horizons is also atypical. However, the interlayering of wacke and mudstone, and the presence of graphite, including significant accumulations, are comparable to rocks of the Burntwood group.

Normalized multi-element profiles for the Burntwood group of the Northeastern Kisseynew subdomain are characterized by shallow positive slopes and variable enrichment at V, Sc, and Cr. The profiles of the Huzyk Creek rocks are notably steeper sloping, with more pronounced enrichments of Ti, V, Sc, and Cr (Figure 17e). The normalized multi-element profiles of Burntwood group rocks from the Snow Lake area have posi-

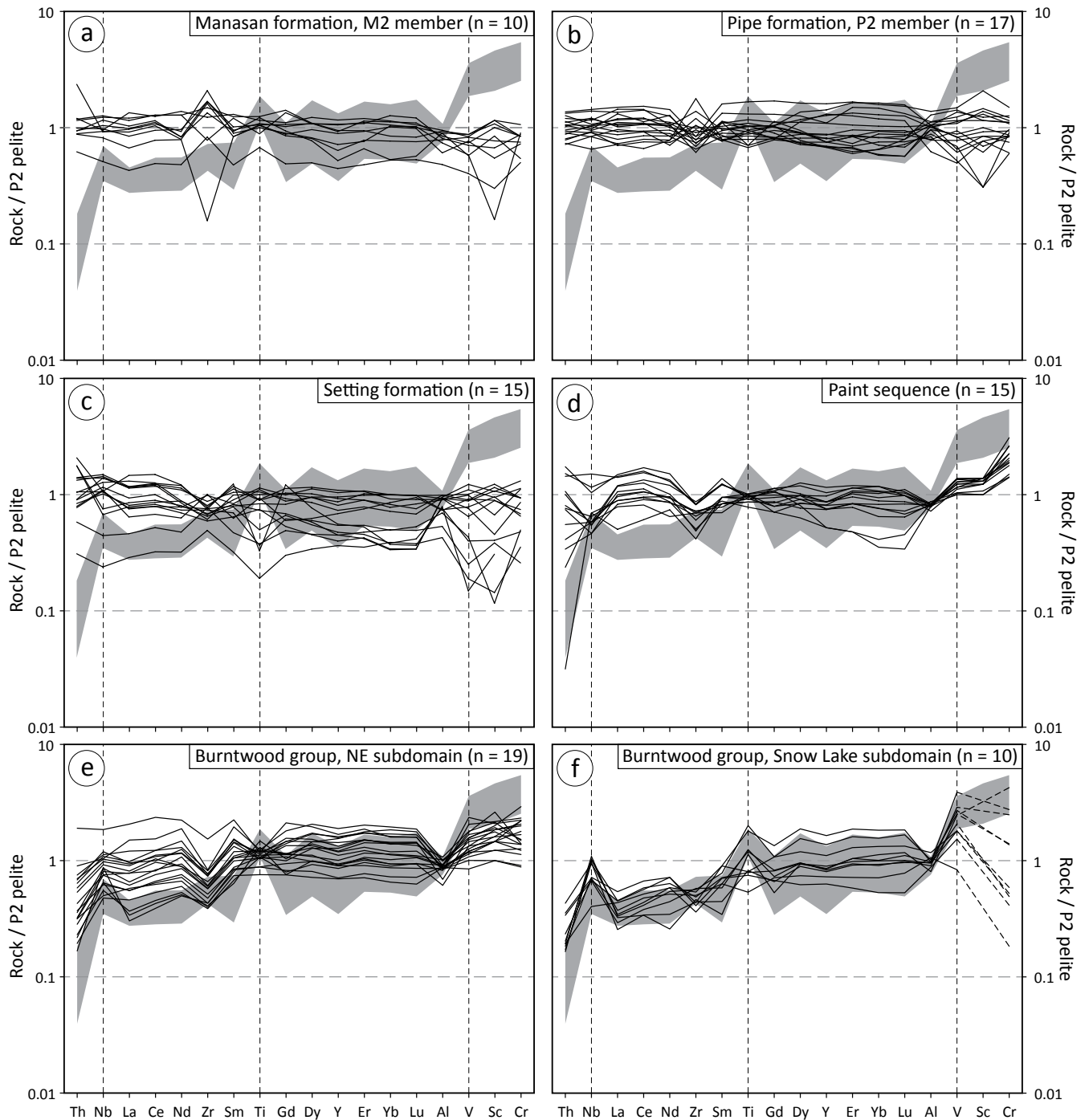


Figure 17: Multi-element diagrams of Thompson nickel belt and Kiseynew domain semipelitic to pelitic rocks, normalized to average P2 pelite of Zwanzig et al. (2007): **a)** Manasan formation, M2 member semipelite; **b)** Pipe formation, P2 member pelite; **c)** Setting formation; **d)** Paint sequence wacke; **e)** Burntwood group rocks from the Northeast Kiseynew subdomain; **f)** Burntwood group rocks from the Snow Lake subdomain. Data sources: Ospwagan group, Appendix 2 and Zwanzig et al. (2007); Paint sequence rocks, Couëslan (2016, unpublished data, 2018); Burntwood group, Appendix 2, Zwanzig et al. (2007), and Zwanzig and Bailes (2010).

tive slopes similar to the Huzyk Creek wacke-mudstones (Figure 17f). The Snow Lake rocks are also characterized by enrichment at Nb, Ti, and V. They differ from the Huzyk Creek rocks in having minor depletion at Zr, and variable Sc and Cr content. The similarity in ϵ_{Nd} values and the overall shape of the multi-element profiles, suggest a similar source for the Burntwood group rocks of the Snow Lake area and the wacke-mudstones of the Huzyk Creek package. The consistently greater enrich-

ment in Ti, Sc, and Cr could indicate a higher contribution of mafic-derived detritus in the Huzyk Creek rocks. An abundance of mafic volcanic-derived detritus in the Huzyk Creek wacke-mudstone sequence could indicate that it was deposited in a sub-basin that was draining an area dominated by mafic volcanic rocks. Burntwood group deposits of the open Kiseynew basin would be subjected to greater homogenization and dilution by other sources of detritus such as the felsic successor-

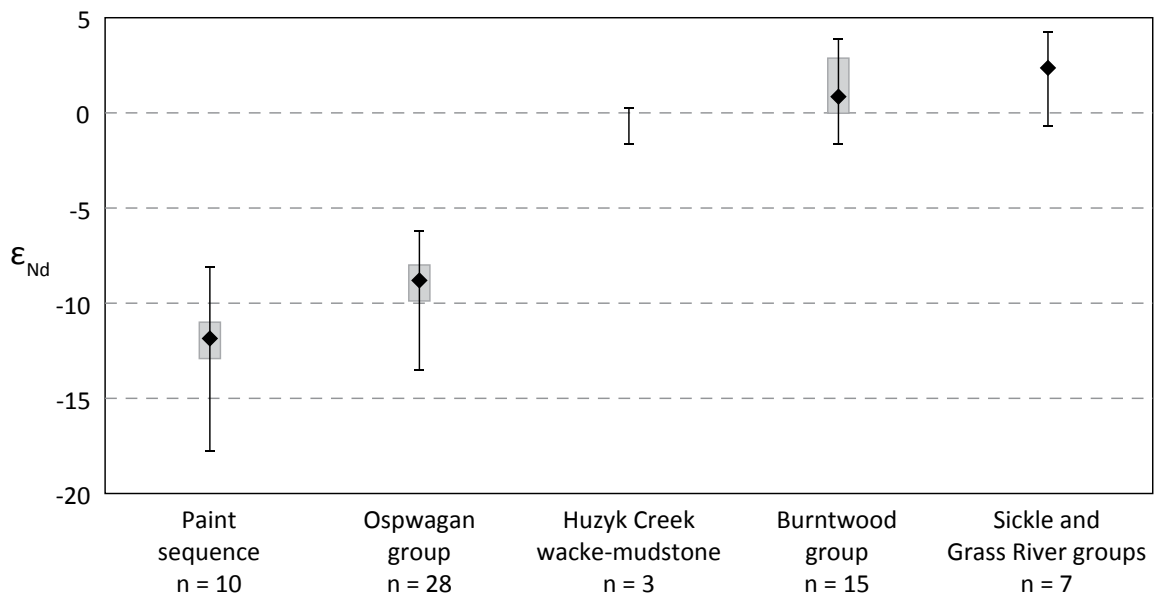


Figure 18: Initial ϵ_{Nd} values for Thompson nickel belt, Kisseynew domain, and Huzyk Creek rocks calculated at 1900 Ma. Black lines indicate the minimum and maximum values for each population, the grey boxes indicate the interquartile range (the middle 50% of the data between the 25th and 75th percentile), and the black diamonds indicate the median value. Data sources: Oswagan, Burntwood, Sickie, and Grass River groups, Böhm et al. (2007); Paint sequence, Couëslan (2016, unpublished data, 2018).

arc intrusions. In addition, the lack of cordierite and sillimanite indicate a lower contribution by aluminous clay minerals. This could suggest that the Huzyk Creek sequence was deposited relatively proximal to the Flin Flon accreted arc terrain, and that a significant proportion of the aluminous clays were transported more distally.

Affinity of the hornblende gneiss and calcsilicate

The hornblende gneiss and calcsilicate are petrographically similar to sequences described along the south, north, and east flanks of the Kisseynew domain (Zwanzig, 2000, 2008; Zwanzig and Bailes, 2010; Couëslan, 2011, unpublished data, 2013). These rocks are interpreted as metabasalts with varying intensities of pre-metamorphic, epidote and carbonate alteration (Zwanzig, 2008). This is in agreement with the geochemical similarities between the hornblende gneiss and calcsilicate, which indicate a common mafic protolith (Figure 8, Figure 19a). The basalt along the flanks of the Kisseynew domain is generally considered older than the Burntwood group and was later thrust into the Kisseynew basin along regional-scale faults, but it may also represent the disrupted basement to the basin (Zwanzig, 2008; Zwanzig and Bailes, 2010). The Huzyk Creek mafic rocks are geochemically similar to fractionated members of the Ponton Lake basalt (Kisseynew domain south flank), which are considered part of the ca. 1900–1880 Ma Amisk collage (Zwanzig and Bailes, 2010; Figure 19b, Figure 20). The Ponton Lake basalt is interpreted as rifted-arc tholeiite, and is characterized by moderately positive ϵ_{Nd} values (+1.2 to +1.3) indicating minor contamination by an older crustal component (Zwanzig and Bailes, 2010). The Huzyk Creek mafic rocks are also geochemically similar to members of the Missi-age (ca. 1850–1830 Ma) Kississing River and Ferro Mine basalts

of the Kisseynew south flank and eastern Snow Lake subdomain, respectively (Gordon and Lemkow, 1987; Zwanzig and Bailes, 2010; Figure 19c, d, Figure 20). The Kississing River and Ferro Mine volcanic rocks are considered transitional between volcanic-arc and continental basalt and may indicate an influx of primitive magma during block faulting and sedimentation in the Missi basin. A sample of Kississing River basalt yielded an ϵ_{Nd} value of +3.7, indicating little to no contamination by an older crustal component (Zwanzig and Bailes, 2010).

The affinity of the Huzyk Creek mafic rocks has implications for the interpretation of the drillcore stratigraphy. If the Huzyk Creek mafic rocks are related to the Amisk collage, it could imply they were faulted into contact with the wacke-mudstone sequence. Alternatively, older Amisk collage rocks could be the basement to the wacke-mudstone package. In either scenario, the interleaving of sedimentary and mafic rocks in drillhole HZ-19-1 would be the result of tectonic repetition. If the Huzyk Creek mafic rocks are Missi-age successor-arc basalt, the interleaving of sedimentary and mafic rocks in drillhole HZ-19-1 could be stratigraphic. The transitional character of the Huzyk Creek mafic rocks between tholeiitic and calcalkaline compositions and their affinity towards continental magmatism (Figure 20) are more indicative of the latter. This may be supported by the ϵ_{Nd} value for the Huzyk Creek hornblende gneiss (+2.7), which is closer to that of the Kississing River basalt (+3.7) than the Ponton Lake basalt (+1.2 to +1.3), and similar to other Missi group basalt and basaltic andesite (+3.2 to +3.8; Zwanzig and Bailes, 2010).

Depositional model and economic considerations

Assembly of the Flin Flon domain intraoceanic arc-collage and its progressive collision with the Sask craton generated

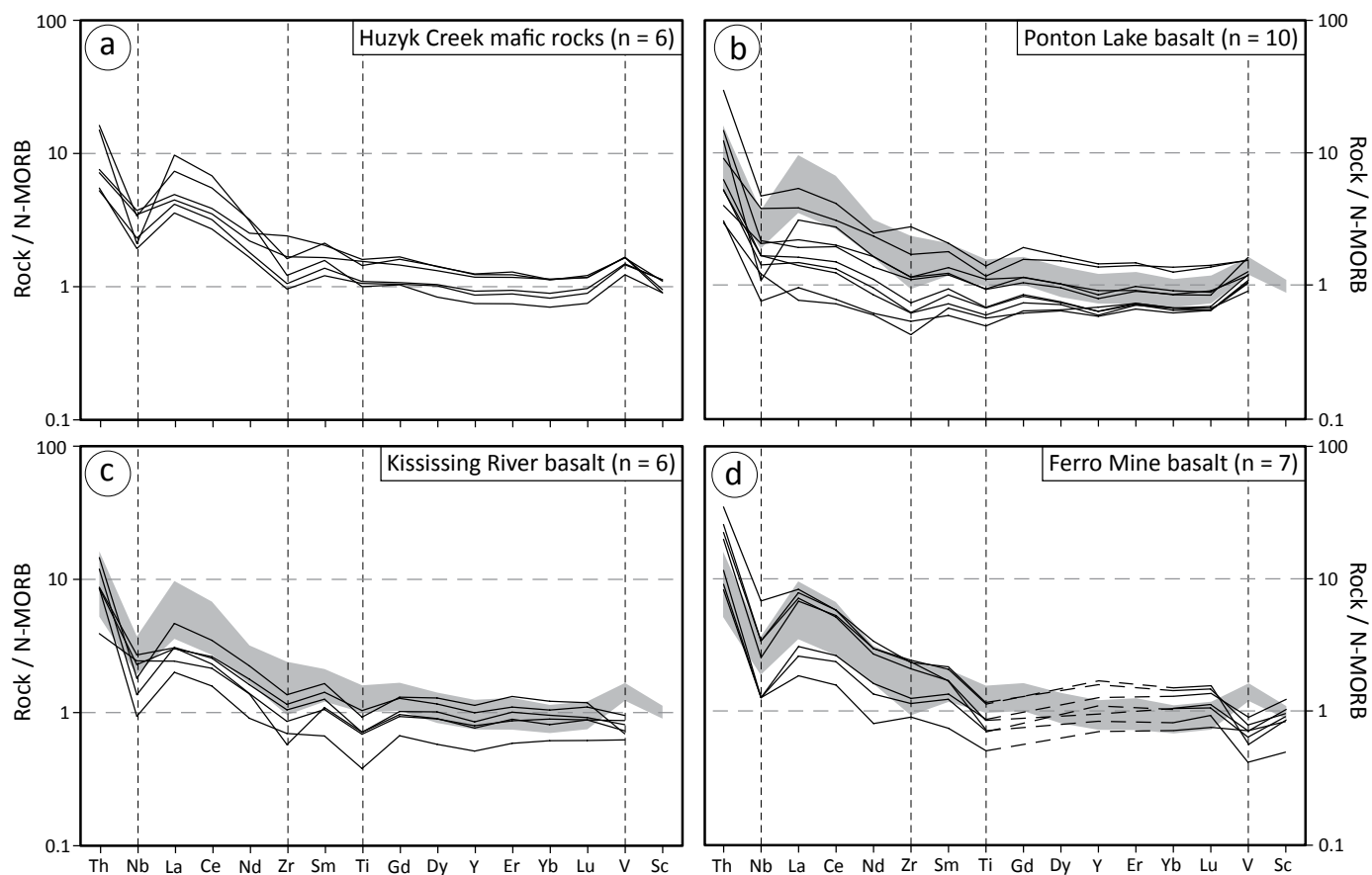


Figure 19: N-MORB-normalized multi-element diagrams of the Huzyk Creek mafic rocks (a) and geochemically similar mafic rocks from the Flin Flon domain (b–d). The grey fields in (b–d) indicate the composition of the Huzyk Creek mafic rocks. Data sources: Ponton Lake and Kississing River basalts, Zwanzig and Bailes (2010); Ferro Mine basalt, Gordon and Lemkow (1987). Abbreviation: N-MORB, normal mid-ocean-ridge basalt.

a volcano-plutonic highland characterized by episodic uplift and high rates of erosion (Stauffer, 1990; David et al., 1996; Zwanzig and Bailes, 2010). Such environments are also subject to high rates of chemical weathering. The waters of river systems draining such terrains contain some of the highest recorded dissolved vanadium concentrations (Gardner et al., 2017). Evidence for this in the Flin Flon domain is provided by the paleosol that locally underlies Missi group conglomerate near Flin Flon. The paleosol forms a weathering profile up to several meters thick with evidence that it developed in an oxygenated atmosphere (Holland et al., 1989; Stauffer, 1990; Pan and Stauffer, 2000; Babechuk and Kamber, 2013; Sindol et al., 2020). Vanadium is a redox sensitive element that is often used to infer paleo-redox conditions (Gardner et al., 2017). In its reduced state (V^{3+}) it is immobile under most conditions, while in its oxidized state (V^{4+} , V^{5+}) it can be mobile in aqueous fluids (Breit and Wanty, 1991). Sindol et al. (2020) suggest V was mobile within the Flin Flon paleosol during initial to intermediate stages of weathering, while Murakami et al. (2016) suggest that V was removed from the system during more advanced weathering. As a test, two pairs of paleosol and least weathered basalt samples were collected from the Flin Flon area in 2019 with the intention to compare V abundances within each set (Appendix 2). Basalt samples were collected 8–10 m below

the paleosol and are assumed to be relatively unweathered. The paleosol samples were collected as close as possible to the top of the weathered horizon. Although the sample set is limited, both instances show depletions of V relative to Al (which is considered to be immobile) in the paleosol compared to the unweathered basalt (Figure 21). The evidence suggests that V was being leached from mafic rocks during chemical weathering, and could have been available for transportation by surface run-off as dissolved V^{5+} . Work by Dessert et al. (2003) suggests that basalt chemical weathering rates are closely related to temperature and run-off. Paleomagnetic studies in the Flin Flon domain suggest it was likely near the paleo-equator at the time of paleosol formation and Missi deposition (Pan and Stauffer, 2000). Average temperatures would therefore have been relatively high and would have promoted higher weathering rates. If the Huzyk Creek mafic rocks represent Missi-age volcanic rocks, this would suggest contemporaneous mafic magmatism, which would be more susceptible to chemical weathering (Gardner et al., 2017).

In an oxygenated atmosphere, V^{5+} would likely remain soluble in the river systems draining the accreted-arc terrain of the Flin Flon domain. Missi group sediments that were deposited in these systems are characterized by abundant iron oxides, and are considered redbed deposits (Stauffer, 1990). In

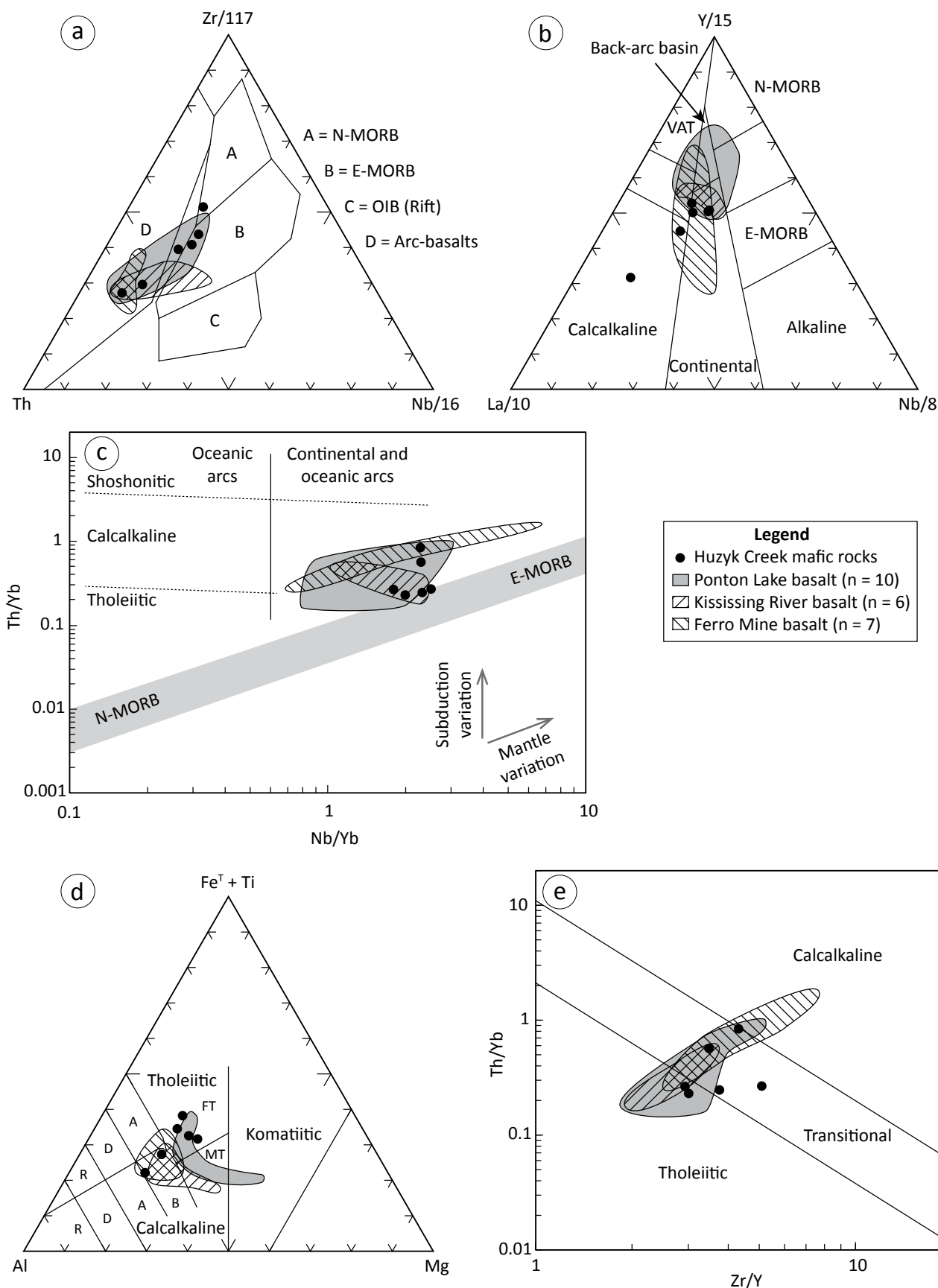


Figure 20: Discrimination diagrams comparing the Huzyk Creek mafic rocks with geochemically similar mafic rocks from the Flin Flon domain: **a)** Th-Zr-Nb diagram of Wood (1980); **b)** La-Y-Nb diagram of Cabanis and Lecolle (1989); **c)** Th/Yb-Nb/Yb diagram of Anderson (2008; modified after Pearce and Peate, 1995); **d)** Al-Fe^T+Ti-Mg diagram of Jensen and Pyke (1982); **e)** Th/Yb-Zr/Y diagram of Ross and Bédard (2009). Abbreviations: A, andesite; B, basalt; D, dacite; E-MORB, enriched mid-ocean-ridge basalt; FT, high-iron tholeiite; MT, high-magnesium tholeiite; N-MORB, normal mid-ocean-ridge basalt; OIB, oceanic-island basalt; R, rhyolite; VAT, volcanic-arc tholeiite.

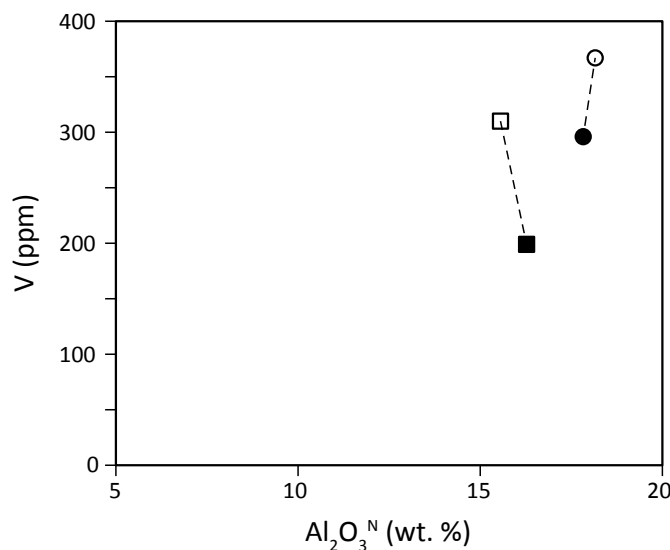


Figure 21: $V\text{-}Al_2O_3^N$ diagram of basalt-paleosol pairs collected in the Flin Flon area. Aluminum oxide is normalized with major elements totaling 100%. Filled symbols represent paleosol compositions, open symbols represent least weathered basalt compositions.

contrast, the coeval marine deposits of the Burntwood group are characterized by disseminated graphite and iron sulphide, indicating deposition in an anoxic or reducing environment. Discharge of the oxygenated waters draining the accreted-arc terrain into the anoxic Kiseynew basin would have resulted in an abrupt change in redox conditions (Figure 22). Shallow and surface waters in the Kiseynew basin were likely oxygenated and able to support planktonic life. Evidence for this is provided by locally magnetite-bearing deposits that are interpreted to be the shoreface transition between the marine Burntwood group and terrestrial Grass River group rocks near the TNB margin, southwest of Setting Lake (Zwanzig et

al., 2007). Similar shoreface deposits occur in the Burntwood group along the Kiseynew domain south flank (Zwanzig and Bales, 2010). The presence of organic matter in the Kiseynew basin would have promoted the reduction of V^{5+} to V^{4+} , which would be readily adsorbed to the organic particles. Moreover, the mixing of oxygenated V^{5+} -enriched waters with the anoxic waters that made up most of the Kiseynew basin water column would have promoted the reduction of V^{5+} to V^{4+} , which would be readily adsorbed to any organic particles settling through the water column. If the Huzyk Creek rocks were deposited in a sub-basin with restricted water circulation, this would have further increased the potential for interaction between V-enriched waters and settling organic particles. Scott et al. (2017) suggest that the hyper-enrichment of V (>500 ppm) in black shales indicates euxinic conditions, which are believed to have occurred at mid-depths (at least periodically) in the oceans at this time (Poulton and Canfield, 2011). Settling of the organic matter into euxinic waters would have further reduced and essentially fixed the adsorbed vanadium as relatively immobile V^{3+} in organic complexes or authigenic clays. Upon burial and metamorphism, the organic matter was transformed into graphite. Thick, organic-rich deposits would be required to form the substantial graphite-rich horizons present at Huzyk Creek and other parts of the Kiseynew domain (e.g. Callinex Mines Incorporated, 2014). Under euxinic conditions, significant additional organic matter could have been contributed by sulphur-oxidizing bacteria along the sediment-water interface (Scott et al., 2017).

A feature of this model is the relatively quick removal of V as it entered the Kiseynew basin. This implies that V would be fractionated from the water column in relative close proximity to the basin margin, and possibly in relative close proximity to the point of fluvial discharge. A similar model has been proposed

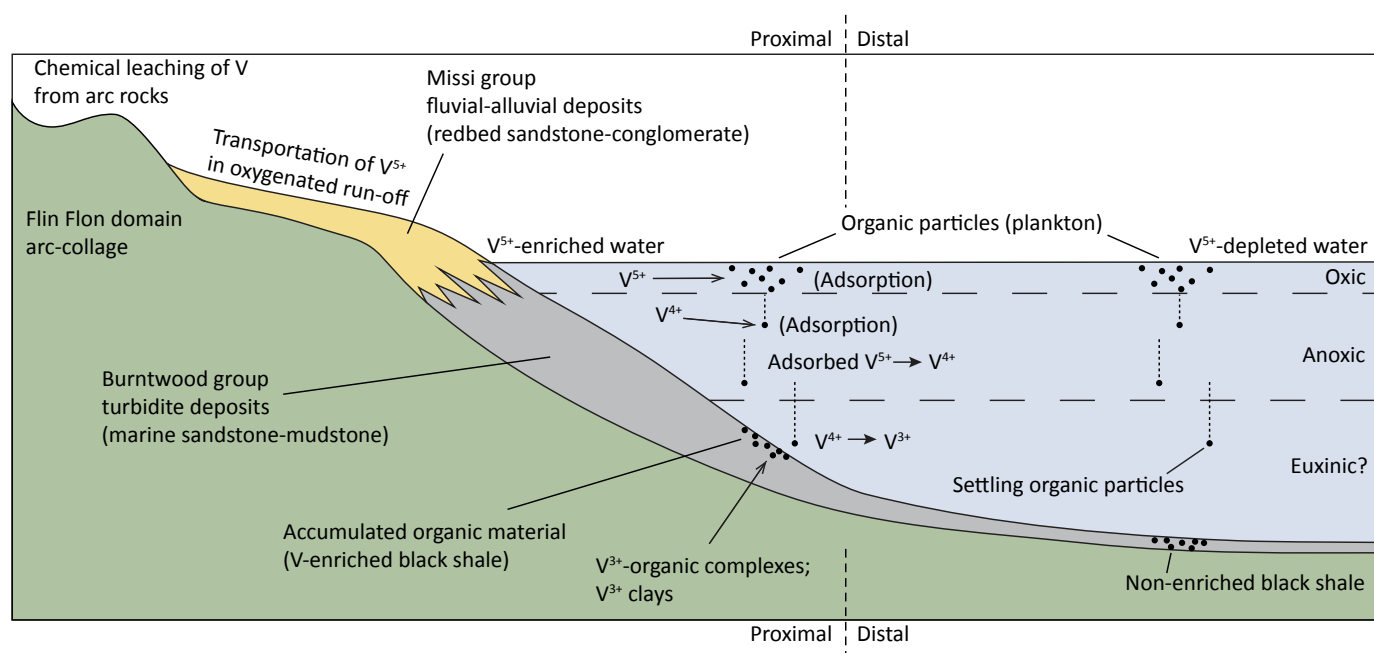


Figure 22: Schematic model for V-enrichment process in the Kiseynew basin.

for the Mo-U-V-enriched Mecca Quarry Shale member of the Midwest United States (Coveney and Martin, 1983; Coveney et al., 1987) and Early Silurian U-enriched shales of the peri-Gondwana shelf (Romer and Cuney, 2018; Romer and Kroner, 2019). Therefore, graphite-rich horizons in close proximity to the Flin Flon (and potentially Lynn Lake) domain margin may have the greatest potential to host V mineralization. This is consistent with additional V-enriched graphite mineralization in the Hargrave–Mitsis rivers area of the sub-Phanerozoic Kiseeynew domain (K. Reid, pers. comm., 2020). It is also consistent with a lack of V-enrichment associated with graphitic samples in the Russell Lake area (Kiseeynew north flank; Martins and Couëslan, 2020) and at the Neuron claim graphite deposit (Northeastern Kiseeynew subdomain; J. Roozendaal, pers. comm., 2020), which were both deposited distally to accreted-arc terranes.

Acknowledgments

The author thanks K. George and I. Robinson for their assistance in the field, as well as E. Anderson and M. Schreckenbach for logistical support. T. Martins provided assistance as well as discussions in the field regarding the core and units of the central Kiseeynew domain. Thanks to C. Böhm for reviewing a draft of this paper and T. Booth for assisting with literature searches. Thanks to Gogal Air Services for providing space at their helicopter base in Snow Lake to review the drillcore, and Kinross Gold Corp. for allowing access to the core splitting facility. Thanks to M. Simpson of Vanadian Energy Corp. and T. Tuba for providing access to the drillcore and core logs, and allowing for sampling and an early viewing of the core during drilling in April of 2019.

References

- Anderson, S.D. 2008: Geology of the Rice Lake area, Rice Lake greenstone belt, southeastern Manitoba (parts of NTS 52L13, 52M4); Manitoba Science, Technology, Energy and Mines, Manitoba Geological Survey, Geoscientific Report GR2008-1, 97 p.
- Ansdell, K.M., Lucas, S.B., Connors, K. and Stern, R.A. 1995: Kiseeynew metasedimentary gneiss belt, Trans-Hudson orogen (Canada): back-arc origin and collisional inversion; *Geology*, v. 23, p. 1039–1043.
- Babechuk, M.G. and Kamber, B.S. 2013: The Flin Flon paleosol revisited; *Canadian Journal of Earth Sciences*, v. 50, p. 1223–1243.
- Bailes, A.H. 2015: Geological setting of the Watts River base metal massive sulphide deposit; HudBay Minerals Inc., unpublished internal geological report, 70 p.
- Bailes, A.H. and McRitchie, W.D. 1978: The transition from low to high grade metamorphism in the Kiseeynew sedimentary gneiss belt, Manitoba; *in* Metamorphism in the Canadian Shield, Geological Survey of Canada, Paper 78-10, p. 155–178.
- Beaumont-Smith, C. 2018: Geology report on the Huzyk Creek property, Ponton Manitoba region; NI 43-101 report prepared for Vanadian Energy Corp., 51 p., URL <https://www.sedar.com/search/search_form_pc_en.htm> [June 2019].
- Bleeker, W. 1990: Evolution of the Thompson Nickel Belt and its nickel deposits, Manitoba, Canada; Ph.D. thesis, University of New Brunswick, Fredericton, New Brunswick, 400 p.
- Böhm, C.O., Zwanzig, H.V. and Creaser, R.A. 2007: Sm-Nd isotopic technique as an exploration tool: delineating the northern extension of the Thompson Nickel Belt, Manitoba, Canada; *Economic Geology*, v. 102, p. 1217–1231.
- Breit, G.N. and Warty, R.B. 1991: Vanadium accumulation in carbonaceous rocks: A review of geochemical controls during deposition and diagenesis; *Chemical Geology*, v. 91, p. 83–97.
- Burnham, O.M., Halden, N., Layton-Matthews, D., Leshner, C.M., Liwanag, J., Heaman, L., Hulbert, L., Machado, N., Michalak, D., Pacey, M., Peck, D.C., Potrel, A., Theyer, P., Toope, K. and Zwanzig, H. 2009: CAMIRO project 97E-02, Thompson Nickel Belt: final report, March 2002, revised and updated 2003; Manitoba Science, Technology, Energy and Mines, Manitoba Geological Survey, Open File OF2008-11, 434 p. plus appendices and GIS shape files for use with ArcInfo®.
- Cabanis, B. and Lecolle, M. 1989: Le diagramme La/10-Y/15-Nb/8: un outil pour la discrimination des series volcaniques et la mise en evidence des processus de melange et/ou de contamination crustale; *Comptes Rendus de l'Academie des Sciences*, v. 309, p. 2023–2029.
- Callinex Mines Incorporated 2014: Grades of up to 60.38% carbon graphite confirmed at Callinex' Neuron property; Callinex Mines Incorporated, press release, April 25, 2014, URL <<https://callinex.ca/grades-of-up-to-60-38-carbon-graphite-confirmed-at-callinex-neuron-property/>> [September 2019].
- Chakhmouradian, A.R., Mumin, A.H., Demény, A. and Elliott, B. 2008: Postorogenic carbonatites at Eden Lake, Trans-Hudson Orogen (northern Manitoba, Canada): geological setting, mineralogy and geochemistry; *Lithos*, v. 103, p. 503–526.
- Corrigan, D. and Rayner, N. 2002: Churchill River–Southern Indian Lake targeted geoscience initiative (NTS 64B, 64C, 64G, 64H), Manitoba: update and new findings; *in* Report of Activities 2002, Manitoba Industry, Trade and Mines, Manitoba Geological Survey, p. 144–158.
- Corrigan, D., Pehrsson, S., Wodicka, N. and De Kemp, E. 2009: The Paleoproterozoic Trans-Hudson Orogen: a prototype of modern accretionary processes; *in* Ancient Orogens and Modern Analogues, J.B. Murphy, J.D. Keppie and A.J. Hynes (ed.), Geological Society of London, Special Publication 327, p. 457–479.
- Couëslan, C.G. 2005: Geochemistry and petrology of the Eden Lake carbonatite and associated silicate rocks; M.Sc. thesis, University of Western Ontario, London, Ontario, 201 p.
- Couëslan, C.G. 2011: Geological investigations in the Manasan Falls area, Thompson Nickel Belt, Manitoba (part of NTS 63P12); *in* Report of Activities 2011, Manitoba Innovation, Energy and Mines, Manitoba Geological Survey, p. 86–93.
- Couëslan, C.G. 2016: Geology of the Paint and Phillips lakes area, Thompson nickel belt, central Manitoba (parts of NTS 63O1, 8, 9, 63P5, 12); Manitoba Growth, Enterprise and Trade, Manitoba Geological Survey, Geoscientific Report GR2016-1, 44 p. and 1 colour map at 1:50 000 scale.
- Couëslan, C.G. 2018a: Geology of the Tower Cu-Zn-Ag-Au deposit, sub-Phanerozoic Superior boundary zone, central Manitoba (part of NTS 63G14); Manitoba Growth, Enterprise and Trade, Manitoba Geological Survey, Open File OF2018-4, 38 p.
- Couëslan, C.G. 2018b: Re-examination of drillcore from southern Phillips Lake, and the possibility of a new nickel-mineralization-hosting sequence in the Thompson nickel belt, central Manitoba (part of NTS 63O1); *in* Report of Activities 2018, Manitoba Growth, Enterprise and Trade, Manitoba Geological Survey, p. 1–16.
- Couëslan, C.G. and Pattison, D.R.M. 2012: Low-pressure regional amphibolite-facies to granulite-facies metamorphism of the Paleoproterozoic Thompson Nickel Belt, Manitoba; *Canadian Journal of Earth Sciences*, v. 49, p. 1117–1153.

- Coveney, R.M., Jr. and Martin, S.P. 1983: Molybdenum and other heavy metals of the Mecca Quarry and Logan Quarry shales; *Economic Geology*, v. 78, p. 132–149.
- Coveney, R.M., Jr., Leventhal, J.S., Glascock, M.D. and Hatch, J.R. 1987: Origins of metals and organic matter in the Mecca Quarry Shale Member and stratigraphically equivalent beds across the Midwest; *Economic Geology*, v. 82, p. 915–933.
- David, J., Bailes, A.H. and Machado, N. 1996: Evolution of the Snow Lake portion of the Palaeoproterozoic Flin Flon and Kiseynew belts, Trans-Hudson Orogen, Manitoba, Canada; *Precambrian Research*, v. 80, no. 1–2, p. 107–124.
- de Capitani, C. and Brown, T.H. 1987: The computation of chemical equilibrium in complex systems containing non-ideal solutions; *Geochimica et Cosmochimica Acta*, v. 51, no. 10, p. 2639–2652.
- de Capitani, C. and Petrakakis, K. 2010: The computation of equilibrium assemblage diagrams with Theriak/Domino software; *American Mineralogist*, v. 95, p. 1006–1016.
- Dessert, C., Dupré, B., Gaillardet, J., François, L.M. and Allègre, C.J. 2003: Basalt weathering laws and the impact of basalt weathering on the global carbon cycle; *Chemical Geology*, v. 202, p. 257–273.
- Diener, J.F.A., Powell, R., White, R.W. and Holland, T.J.B. 2007: A new thermodynamic model for clino- and orthoamphiboles in the system $\text{Na}_2\text{O}-\text{CaO}-\text{FeO}-\text{MgO}-\text{Al}_2\text{O}_3-\text{SiO}_2-\text{H}_2\text{O}-\text{O}$; *Journal of Metamorphic Geology*, v. 25, no. 6, p. 631–656.
- Gardner, C.B., Carey, A.E., Lyons, W.B., Goldsmith, S.T., McAdams, B.C. and Trierweiler, A.M. 2017: Molybdenum, vanadium, and uranium weathering in small mountainous rivers and rivers draining high-standing islands; *Geochimica et Cosmochimica Acta*, v. 219, p. 22–43.
- Goldstein, S.L., O’Nions, R.K. and Hamilton, P.J. 1984: A Sm-Nd study of atmospheric dusts and particulates from major river systems; *Earth and Planetary Science Letters*, v. 70, p. 221–236.
- Gordon, T.M. 1989: Thermal evolution of the Kiseynew sedimentary gneiss belt, Manitoba: metamorphism at an early Proterozoic accretionary margin; in *Evolution of Metamorphic Belts*, J.S. Daly, R.A. Cliff and B.W.D. Yardley (ed.), Geological Society, Special Publication 43, p. 233–243.
- Gordon, T.M. and Lemkow, D.R. 1987: Geochemistry of Missi group volcanic rocks, Wekusko Lake, Manitoba; Geological Survey of Canada, Open File 1442, 38 p.
- Gordon, T.M., Hunt, P.A., Bailes, A.H. and Syme, E.C. 1990: U-Pb ages from the Flin Flon and Kiseynew belts, Manitoba: chronology of crust formation at an Early Proterozoic accretionary margin; in *The Early Proterozoic Trans-Hudson Orogen of North America*, J.F. Lewry and M.R. Stauffer (ed.), Geological Association of Canada, Special Paper 37, p. 177–199.
- Growdon, M.L. 2010: Crustal development and deformation of Laurentia during the Trans-Hudson and Alleghenian orogenies; Ph.D. thesis, Indiana University, Bloomington, Indiana, 237 p.
- Heaman, L.M., Böhm, C.O., Machado, N., Krogh, T.E., Weber, W. and Corkery, M.T. 2011: The Pikwitonei Granulite Domain, Manitoba: a giant Neoarchean high-grade terrane in the northwest Superior Province; *Canadian Journal of Earth Sciences*, v. 48, p. 205–245.
- Holland, T.J.B. and Powell, R. 1998: An internally consistent thermodynamic data set for phases of petrological interest; *Journal of Metamorphic Geology*, v. 16, no. 3, p. 309–343.
- Holland, H.D., Feakes, C.R. and Zbinden, E.A. 1989: The Flin Flon paleosol and the composition of the atmosphere 1.8 BYBP; *American Journal of Science*, v. 289, p. 362–389.
- Holness, M.B. and Sawyer, E.W. 2008: On the pseudomorphing of melt-filled pores during the crystallization of migmatites; *Journal of Petrology*, v. 49, p. 1343–1363.
- Holness, M.B., Cesare, B. and Sawyer, E.W. 2011: Melted rocks under the microscope: microstructures and their interpretation; *Elements*, v. 7, p. 247–252.
- Hubregtse, J.J.M.W. 1980: The Archean Pikwitonei granulite domain and its position at the margin of the northwestern Superior Province (central Manitoba); Manitoba Department of Energy and Mines, Mineral Resources Division, Geological Paper GP80-3, 16 p.
- Jensen, L.S. and Pyke, D.R. 1982: Komatiites in the Ontario portion of the Abitibi belt; in *Komatiites*, N.T. Arndt and E.G. Nisbet (ed.), George Allen and Unwin, London, United Kingdom, p. 147–157.
- Kelley, K.D., Scott, C.T., Polyak, D.E. and Kimball, B.E. 2017: Vanadium; in *Critical Mineral Resources of the United States—Economic and Environmental Geology and Prospects for Future Supply*, K.J. Schulz, J.H. DeYoung, Jr., R.R. Seal, II and D.C. Bradley (ed.), U.S. Geological Survey, Professional Paper 1802, p. U1–U36.
- Leclair, A.D., Lucas, S.B., Broome, H.J., Viljoen, D.W. and Weber, W. 1997: Regional mapping of Precambrian basement beneath Phanerozoic cover in southeastern Trans-Hudson Orogen, Manitoba and Saskatchewan; *Canadian Journal of Earth Sciences*, v. 34, p. 618–634.
- Lewry, J.F., Thomas, D.J., Macdonald, R. and Chiarenzelli, J. 1990: Structural relations in accreted terranes of the Trans-Hudson Orogen, Saskatchewan: telescoping in a collisional regime?; in *The Early Proterozoic Trans-Hudson Orogen of North America*, J.F. Lewry and M.R. Stauffer (ed.), Geological Association of Canada, Special Paper 37, p. 75–94.
- Machado, N., Zwanig, H.V. and Parent, M. 1999: U-Pb ages of plutonism, sedimentation, and metamorphism of the Paleoproterozoic Kiseynew metasedimentary belt, TransHudson Orogen (Manitoba, Canada); *Canadian Journal of Earth Sciences*, v. 36, p. 1829–1842.
- Martins, T. 2012: Whole-rock geochemistry of the Burntwood Lake alkali-feldspar syenite, west-central Manitoba (part of NTS 63N8); Manitoba Innovation, Energy and Mines, Manitoba Geological Survey, Data Repository Item DRI2012001, Microsoft® Excel® file.
- Martins, T. 2016a: Rare metals in Manitoba: Brezden Lake intrusive complex; Manitoba Growth, Enterprise and Trade, Manitoba Geological Survey, URL <<https://www.gov.mb.ca/iem/geo/raremetals/pdfs/brezden.pdf>> [March 2020].
- Martins, T. 2016b: Rare metals in Manitoba: Burntwood Lake intrusive complex; Manitoba Growth, Enterprise and Trade, Manitoba Geological Survey, URL <<https://www.gov.mb.ca/iem/geo/raremetals/pdfs/burntwood.pdf>> [March 2020].
- Martins, T. 2016c: Rare metals in Manitoba: Eden Lake carbonatite complex; Manitoba Growth, Enterprise and Trade, Manitoba Geological Survey, URL <<https://www.gov.mb.ca/iem/geo/raremetals/pdfs/edenlake.pdf>> [March 2020].
- Martins, T. and Couëslan, C.G. 2019: Geological investigations in the Russell–McCallum lakes area, northwestern Manitoba (parts of NTS 64C3–6); in *Report of Activities 2019*, Manitoba Agriculture and Resource Development, Manitoba Geological Survey, p. 30–41.
- Martins, T. and Couëslan, C.G. 2020: Whole-rock geochemistry of the Russell Lake mapping project, northwestern Manitoba (parts of NTS 64C3–6); Manitoba Agriculture and Resource Development, Manitoba Geological Survey, Data Repository Item DRI2020001, Microsoft® Excel® file.
- Martins, T., Couëslan C.G. and Böhm, C.O. 2012: Rare metals scoping study of the Brezden Lake intrusive complex, western Manitoba (part of NTS 64C4); Manitoba Innovation, Energy and Mines, Manitoba Geological Survey, Data Repository Item DRI2012006, Microsoft® Excel® file.
- McDonough, W.F. and Sun, S.-S. 1995: The composition of the Earth; in *Chemical Evolution of the Mantle*, W.F. McDonough, N.T. Arndt and S. Shirey (ed.), *Chemical Geology*, v. 120, p. 223–253.

- Mezger, K., Bohlen, S.R. and Hanson, G.N. 1990: Metamorphic history of the Archean Pikwitonei granulite domain and the Cross Lake subprovince, Superior Province, Manitoba, Canada; *Journal of Petrology*, v. 31, p. 483–517.
- Murakami, T., Matsuura, K. and Kanzaki, Y. 2016: Behaviors of trace elements in Neoarchean and Paleoproterozoic paleosols: implications for atmospheric oxygen evolution and continental oxidative weathering; *Geochimica et Cosmochimica Acta*, v. 192, p. 203–219.
- Pan, Y. and Stauffer, M.R. 2000: Cerium anomaly and Th/U fractionation in the 1.85 Ga Flin Flon Paleosol: clues from REE- and U-rich accessory minerals and implications for paleoatmospheric reconstruction; *American Mineralogist*, v. 85, p. 898–911.
- Pattison, D.R.M., Chacko, T., Farquhar, J. and McFarlane, C.R.M. 2003: Temperatures of granulite-facies metamorphism: constraints from experimental phase equilibria and thermobarometry corrected for retrograde exchange; *Journal of Petrology*, v. 44, p. 867–900.
- Pattison, D.R.M. and Tinkham, D.K. 2009: Interplay between equilibrium and kinetics in prograde metamorphism of pelites: an example from the Nelson aureole, British Columbia; *Journal of Metamorphic Geology*, v. 27, p. 249–279.
- Pearce, J.A. 1996: A user's guide to basalt discrimination diagrams; in *Trace Element Geochemistry of Volcanic Rocks: Applications for Massive Sulphide Exploration*, D.A. Wyman (ed.), Geological Association of Canada, Short Course Notes, no. 12, p. 79–113.
- Pearce, J.A. and Peate, D.W. 1995: Tectonic implications of the composition of volcanic arc magmas; *Annual Review of Earth and Planetary Sciences*, v. 23, p. 251–285.
- Poulton, S.W. and Canfield, D.E. 2011: Ferruginous conditions: a dominant feature of the ocean through Earth's history; *Elements*, v. 7, no. 2, p. 107–112.
- Rayner, N. and Percival, J.A. 2007: Uranium-lead geochronology of basement units in the Wuskwatim–Tullibee lakes area, north-eastern Kiseeynew Domain, Manitoba (NTS 630); in *Report of Activities 2007*, Manitoba Science, Technology, Energy and Mines, Manitoba Geological Survey, p. 82–90.
- Reid, K.D. 2018: Sub-Phanerozoic basement geology from drillcore observations in the Watts, Mitishto and Hargrave rivers area, eastern Flin Flon belt, west-central Manitoba (parts of NTS 63J5, 6, 11, 12, 13, 14); in *Report of Activities 2018*, Manitoba Growth, Enterprise and Trade, Manitoba Geological Survey, p. 37–47.
- Robinson, G.R., Jr., Hammarstrom, J.M. and Olson, D.W. 2017: Graphite; in *Critical Mineral Resources of the United States—Economic and Environmental Geology and Prospects for Future Supply*, K.J. Schulz, J.H. DeYoung, Jr., R.R. Seal, II and D.C. Bradley (ed.), United States Geological Survey, Professional Paper 1802, p. J1–J24.
- Romer, R.L. and Cuney, M. 2018: Phanerozoic uranium mineralization in Variscan Europe – more than 400 Ma of tectonic, supergene, and climate-controlled uranium redistribution; *Ore Geology Reviews*, v. 102, p. 474–504.
- Romer, R.L. and Kroner, U. 2019: First direct evidence for a contiguous Gondwana shelf to the south of the Rheic Ocean; *Geology*, v. 47, p. 767–770.
- Ross, P.-S. and Bédard, J.H. 2009: Magmatic affinity of modern and ancient subalkaline volcanic rocks determined from trace-element discriminant diagrams; *Canadian Journal of Earth Sciences*, v. 46, p. 823–839.
- Sawyer, E.W. 2008: Atlas of migmatites; *The Canadian Mineralogist*, Special Publication 9, 371 p.
- Schmidberger, S.S., Simonetti, A., Heaman, L.M., Creaser, R.A. and Whiteford, S. 2007: Lu–Hf, in-situ Sr and Pb isotope and trace element systematics for mantle eclogites from the Diavik diamond mine: evidence for Paleoproterozoic subduction beneath the Slave craton, Canada; *Earth and Planetary Science Letters*, v. 254, p. 55–68.
- Scott, C., Slack, J.F. and Kelley, K.D. 2017: The hyper-enrichment of V and Zn in black shales of the Late Devonian–Early Mississippian Bakken Formation (USA); *Chemical Geology*, v. 452, p. 24–33.
- Simard, R.-L., McGregor, C.R., Rayner, N. and Creaser, R.A. 2010: New geological mapping, geochemical, Sm–Nd isotopic and U–Pb age data for the eastern sub-Phanerozoic Flin Flon Belt, west-central Manitoba (parts of NTS 63J3–6, 11, 12, 14, 63K1–2, 7–10); in *Report of Activities 2010*, Manitoba Innovation, Energy and Mines, Manitoba Geological Survey, p. 69–87.
- Sindol, G.P., Babechuk, M.G., Petrus, J.A. and Kamber, B.S. 2020: New insights into Paleoproterozoic surficial conditions revealed by 1.85 Ga corestone-rich saprolith; *Chemical Geology*, v. 545, article 119621, URL <<https://doi.org/10.1016/j.chemgeo.2020.119621>> [June 2020].
- Stauffer, M.R. 1990: The Missi Formation: an Aphebian molasse deposit in the Reindeer Lake zone of the Trans-Hudson orogen, Canada; in *The Early Proterozoic Trans-Hudson Orogen of North America*, J.F. Lewry and M.R. Stauffer (ed.), Geological Association of Canada, Special Paper 37, p. 121–141.
- Tinkham, D.K. and Ghent, E.D. 2005: Estimating P–T conditions of garnet growth with isochemical phase-diagram sections and the problem of effective bulk-composition; *The Canadian Mineralogist*, v. 43, p. 35–50.
- United States Geological Survey 2017: Critical mineral resources of the United States—economic and environmental geology and prospects for future supply; K.J. Schulz, J.H. DeYoung, Jr., R.R. Seal, II and D.C. Bradley (ed.), United States Geological Survey, Professional Paper 1802, 797 p.
- Unterschutz, J.L.E., Creaser, R.A., Erdmer, P., Thompson, R.I. and Daughtry, K.L. 2002: North American margin origin of Quesnel terrane strata in the southern Canadian Cordillera: inferences from geochemical and Nd isotopic characteristics of Triassic metasedimentary rocks; *Geological Society of America Bulletin*, v. 114, p. 462–475.
- Vanadian Energy Corporation 2019: Vanadian Energy intersects 0.22% V₂O₅ over 9.74 metres on the Huzyk Creek property; Vanadian Energy Corporation, press release, May 21, 2019, URL <<https://www.vanadianenergy.com/NR-2019-05-21-Drilling-results.pdf>> [June 2019].
- Waters, D.J. 2001: The significance of prograde and retrograde quartz-bearing intergrowth microstructures in partially melted granulite-facies rocks; *Lithos*, v. 56, p. 97–110.
- White, D.J., Lucas, S.B., Bleeker, W., Hajnal, Z., Lewry, J.F. and Zwanzig, H.V. 2002: Suture-zone geometry along an irregular Paleoproterozoic margin: the Superior boundary zone, Manitoba, Canada; *Geology*, v. 30, p. 735–738.
- White, R.W., Powell, R. and Holland, T.J.B. 2001: Calculation of partial melting equilibria in the system Na₂O–CaO–K₂O–FeO–MgO–Al₂O₃–SiO₂–H₂O (NCKFMASH); *Journal of Metamorphic Geology*, v. 19, p. 139–153.
- White, R.W., Powell, R. and Clarke, G.L. 2002: The interpretation of reaction textures in Fe-rich metapelitic granulites of the Musgrave Block, central Australia: constraints from mineral equilibria calculations in the system K₂O–FeO–MgO–Al₂O₃–SiO₂–H₂O–TiO₂–Fe₂O₃; *Journal of Metamorphic Geology*, v. 20, p. 41–55.
- White, R.W., Powell, R. and Holland, T.J.B. 2007: Progress relating to calculation of partial melting equilibria for metapelites; *Journal of Metamorphic Geology*, v. 25, p. 511–527.
- Winchester, J.A., Park, R.G. and Holland, J.G. 1980: The geochemistry of Lewisian semipelitic schists from the Gairloch District, Western Ross; *Scottish Journal of Geology*, v. 16, p. 165–179.
- Wood, D.A. 1980: The application of a Th–Hf–Ta diagram to problems of tectonomagmatic classification and to establishing the nature of crustal contamination of basaltic lavas of the British Tertiary volcanic province; *Earth and Planetary Science Letters*, v. 50, p. 11–30.

- Zwanzig, H.V. 1997: Comments on “Kisseynew metasedimentary gneiss belt, Trans-Hudson orogen (Canada): Back-arc origin and collisional inversion” by Ansdell et al., 1995 (*Geology*, v. 23, p. 1039–1043); *Geology*, v. 25, p. 90–91.
- Zwanzig, H.V. 1998: Structural mapping of the Setting Lake area (parts of NTS 63J/15 and 63O/1, 2); *in* Report of Activities 1998, Manitoba Energy and Mines, Geological Services, p. 40–45.
- Zwanzig, H.V. 1999: Structure and stratigraphy of the south flank of the Kisseynew Domain in the Trans-Hudson Orogen, Manitoba: implications for 1.845–1.77 Ga collision tectonics; *Canadian Journal of Earth Sciences*, v. 36, p. 1859–1880.
- Zwanzig, H.V. 2000: Geochemistry and tectonic framework of the Kisseynew Domain–Lynn Lake Belt Boundary (part of NTS 63P/13); *in* Report of Activities 2000, Manitoba Industry, Trade and Mines, Manitoba Geological Survey, p. 91–96.
- Zwanzig, H.V. 2008: Correlation of lithological assemblages flanking the Kisseynew Domain, Manitoba (parts of NTS 63N, 63O, 64B, 64C): proposal for tectonic/metallogenic subdomains; *in* Report of Activities 2008, Manitoba Science, Technology, Energy and Mines, Manitoba Geological Survey, p. 38–52.
- Zwanzig, H.V. and Bailes, A.H. 2010: Geology and geochemical evolution of the northern Flin Flon and southern Kisseynew domains, Kissinging–File lakes area, Manitoba (parts of NTS 63K, N); Manitoba Innovation, Energy and Mines, Manitoba Geological Survey, Geoscientific Report GR2010-1, 135 p.
- Zwanzig, H.V., Macek, J.J. and McGregor, C.R. 2007: Lithostratigraphy and geochemistry of the high-grade metasedimentary rocks in the Thompson nickel belt and adjacent Kisseynew domain, Manitoba: implications for nickel exploration; *Economic Geology*, v. 102, p. 1197–1216.